Physical Properties of Polymers Handbook

Second Edition

Edited by

James E. Mark

Polymer Research Center and
Department of Chemistry
University of Cincinnati
Cincinnati, Ohio

Springer

CHAPTER 29

Polymer Networks and Gels

Ferenc Horkay* and Gregory B. McKenna†

*National Institutes of Health, National Institute of Child Health and Human Development, Laboratory of Integrative and Medical Biophysics, Section on Tissue Biophysics and Biomimetics, Bethesda, MD 20892
†Department of Chemical Engineering, Texas Tech University, Lubbock, TX 79409-3121

Abstract: When long polymer molecules are chemically linked together to form a three-dimensional network, the resulting material exhibits a unique set of properties that have come to be referred to as "rubberlike." Among these are large deformation elasticity which has important consequences for mechanical behavior and resistance to solvent attack. As for the latter, when solvent molecules penetrate into the polymer it undergoes swelling rather than dissolution, and the diluted network is referred to as a chemically crosslinked gel. A survey of the thermodynamics and mechanics of crosslinked gels is presented. Subjects include the phenomenological description of crosslinked networks within the framework of finite elasticity theory and continuum thermodynamics. Particular emphasis is placed on the Valanis–Landel form of the strain energy density function. Several statistical mechanical models of rubber elasticity are also presented. Of particular usefulness are the affine and phantom network models, which are commonly used to derive information about the molecular parameters of the gel from swelling or mechanical measurements. Techniques for using these models and the more modern Flory–Erman constrained junction model and its most recent modifications are described. The application of Scaling Theory to polymer gels is also considered.

Key Words: Crosslinked Rubber, Flory–Rehner Hypothesis, Gels, Networks, Polymer, Rubber Elasticity, Scaling Theory, Solution Thermodynamics, Swelling, Valanis–Landel Function.

29.1 INTRODUCTION

Polymer networks and gels have a wide range of technical and biological applications. Crosslinked polymers are the building blocks of systems as different as rubber tires and scaffolds for tissue engineering. Morphology, molecular and supermolecular structures play important roles, especially when considering processing and final properties. While such materials have been the subjects of experimental and theoretical investigations for more than six decades, their understanding still presents a challenge. Gels exhibit both solid-like and liquid-like properties. The three-dimensional network structure obtained by joining long flexible polymer strands at junction points is the most important molecular characteristic required to achieve "rubberlike" behavior. Numerous models have been proposed to develop a rigorous molecular description of polymer gels. Statistical mechanical theories along these lines encounter serious mathematical difficulties. Rubber elasticity theories, therefore, omit a detailed description of the conformation of polymer chains. Earlier models focus on the effects of topological constraints on the crosslinks. Modern theories are made more realistic by applying the constraints to other parts of the chains. As a result, it is of great interest and importance to understand the structure–property relationships that determine network and gel behaviors.

To begin, when long polymer molecules are chemically linked together to form a three-dimensional network, the resulting material exhibits a unique set of properties that

have come to be referred to as rubberlike. Among these are large deformation elasticity which has important consequences for mechanical behavior and resistance to solvent attack. As for the latter, when solvent molecules penetrate into the polymer it undergoes swelling rather than dissolution, and the diluted network is referred to as a chemically crosslinked gel. While there are several structures that exhibit gellike behavior, e.g., (1) covalent networks of large chain molecules, (2) physical networks formed by aggregation of polymer chains (gelatin, agarose), (3) lamellar, fibrillar, or reticular systems exhibiting partially ordered structures (clays, surfactants, etc.), the focus of this work is solely on elastomeric polymer networks containing a three-dimensional permanent structure of high molecular weight chain molecules swollen in a low molecular weight diluent as depicted in Fig. 29.1.

The covalent network, composed of long flexible chains capable of adopting large conformational changes (chain deformations), extends throughout the sample providing the ability to undergo large and reversible (elastic) deformations and a corresponding ability to swell rather than dissolve. Though the molecular origins of rubber elasticity were recognized as early as the 1930s and 1940s [1–5], a complete theoretical description of the swelling behavior of rubberlike polymers has yet to be achieved. The result is that, while there is a general understanding of the behavior of crosslinked materials within the framework of some "classical" models of rubber elasticity, there are still several unresolved problems. For example, even the fundamental assumption, originally put forth by Frenkel [5], Flory and Rehner [2,4] that the free energy of mixing of a solvent and rubber network can be separated into an elastic term for the network and a mixing term for the solvent and polymer has been a subject for much research and discussion over the years [6–32].

There is a diversity of theroetical models used to elucidate the relationships between the molecular parameters of the network and the various experimental results [33–57]. Hence, the resulting deduction of the molecular structure of the network can depend on the model chosen for data analysis. Additionally, the structure of the networks at the supermolecular level is a function of the preparation conditions (temperature, concentration at crosslinking, chemical nature of the crosslinker, etc.). During network formation imperfections in the structure may also develop. In many cases the crosslinking process leads to fixation of otherwise nonequilibrium states. A wide variety of molecular superstructures may be produced within networks prepared from the same starting materials. This makes comparisons of experimental results from different literature sources extremely complicated. Consequently, a simple tabulation of previously published data is not particularly useful.

The present work is intended to survey briefly the basic thermodynamic considerations of rubber elasticity and

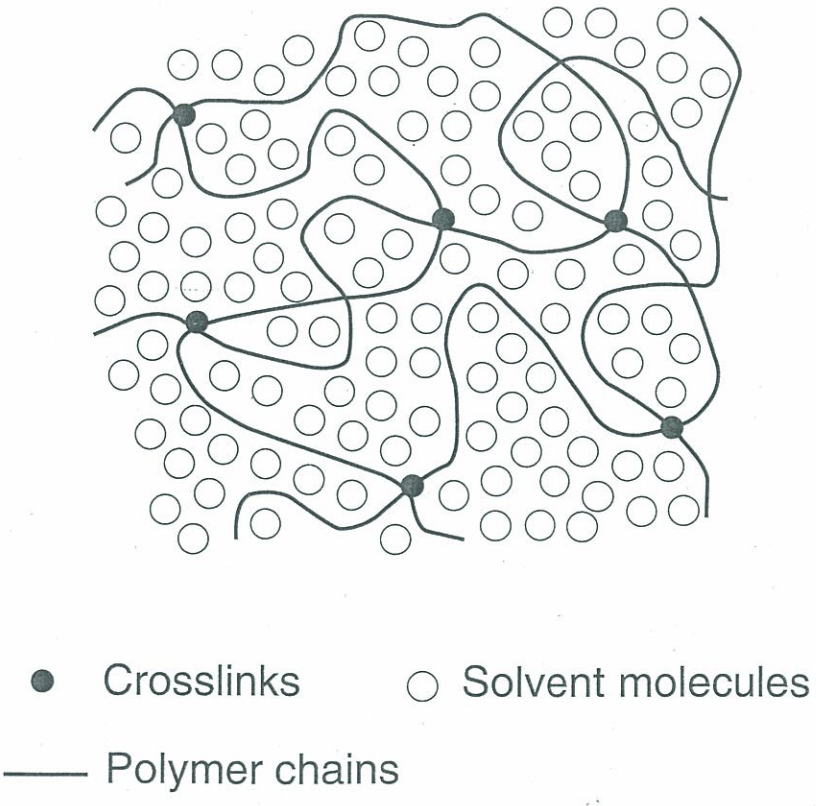

FIGURE 29.1. Schematic representation of a chemically crosslinked polymer network swollen by a low molecular weight solvent.

swelling from both a continuum point of view and with regard to existing network models. Our goal is to illustrate the range of applicability and the limitations of the different approaches for the description of experimental data. The main emphasis is to discuss the structure–property relationships of amorphous polymer networks and gels. We briefly summarize what we believe are the most important ideas of the theories, and compare them with experimental observations made on well-defined networks. For details of each model the reader is referred to the original literature. We focus exclusively on the equilibrium properties of model networks in the dry and swollen states, and the relationships between macroscopically measurable physical quantities. We do not deal with the consequences of the morphology and supermolecular architecture of the polymer network, which can be revealed by scattering measurements. Certain fundamental topics (e.g., effect of charged groups, finite chain extensibility, contribution of filler particles, dynamic properties such as relaxation behavior) are not discussed here.

Additionally, this work should provide the reader with the ability to use the models to obtain estimates of the molecular structure of the gel through analysis and interpretation of typical sets of experimental data. Conversely, the swelling and mechanical responses of new networks should be able to be estimated from a chemist's knowledge of the molecular parameters of the network.

29.2 THEORETICAL BACKGROUND

29.2.1 General Considerations

In thinking about the behavior of rubber networks and gels, there are two features of behavior that we will consider in the following. First, the fundamental nature of the elastomeric network itself in the undiluted state needs to be weighed. This will be done using both the phenomenological theories of rubber elasticity and the molecular (statistical mechanical) models. Both approaches result in forms of the free energy function (Helmholtz) of the network and ultimately need to give the same descriptions of the phenomenological behavior of the dry network. Second, we will consider the specific behavior of the swollen network or gel from similar considerations. In the latter case the formulation of a mixing free energy as a function of the swelling ratio is also required in addition to the elastic free energy. We also remark that the mere presence of the crosslink sites may alter the expressions for the free energy of mixing.

Laboratory measurements, for the most part, record the macroscopic behavior of the material. Depending on the purposes of the experimenter, the link between the molecular models and the phenomenological models provides a basis for either deducing molecular parameters from the measurements or for predicting future measurements from known molecular structures. The latter is primarily important to estimate the physical properties of a given gel whose molecular structure is known. The background provided in what follows should permit one to do both within the limitations of current knowledge.

29.2.2 The Strain Energy Density Function—The Mechanical Contribution to the Helmholtz Free Energy

Continuum Description

There is an extensive body of literature describing the stress–strain response of rubberlike materials that is based upon the concepts of Finite Elasticity Theory which was originally developed by Rivlin and others [58,59]. The reader is referred to this literature for further details of the relevant developments. For the purposes of this paper, we will discuss the developments of the so-called Valanis–Landel strain energy density function, [60] because it is of the form that most commonly results from the statistical mechanical models of rubber networks and has been very successful in describing the mechanical response of crosslinked rubber. It is resultingly very useful in understanding the behavior of swollen networks.

Here we begin with a sample of rubber having initial dimensions l_1, l_2, l_3. We deform it by an amount $\Delta l_1, \Delta l_2, \Delta l_3$ and define the stretch (ratio) in each direction as $\lambda_i = (l_i + \Delta l_i)/l_i = l/l_i$. The purpose of Finite Elasticity Theory has been to relate the deformations of the material to the stresses needed to obtain the deformation. This is done through the strain energy density function, which we will describe using the Valanis–Landel formalism as $W(\lambda_1, \lambda_2, \lambda_3)$. Importantly, as we will see later, this is the mechanical contribution to the Helmholtz free energy. Valanis and Landel assumed [60] that the strain energy density function is a separable function of the stretches λ_i:

$$W(\lambda_1, \lambda_2, \lambda_3) = w(\lambda_1) + w(\lambda_2) + w(\lambda_3) + a \ln(\lambda_1 \lambda_2 \lambda_3). \quad (29.1)$$

While the term $a \ln(\lambda_1\lambda_2\lambda_3)$ is not important in the mechanical response, because of the incompressibility assumption, it may be important in swelling [61]. We also note that some of the molecular models include this logarithmic term. Then, the principal stresses σ_{ii} in any deformation can be related through the strain energy function and deformations as follows:

$$\sigma_{ii} - \sigma_{jj} = \lambda_i\, w'(\lambda_i) - \lambda_j\, w'(\lambda_j), \quad (29.2)$$

where $w'(\lambda) = dw(\lambda)/d\lambda$ is the derivative of the VL function $w(\lambda)$. We note that the stresses are the true stresses in that they are referred to the deformed sample geometry. In the dry, unswollen rubber, the material is generally assumed to be incompressible, meaning that the distortional or shape changing deformations are much more easily made than are the volume changing ones, so the latter are

negligible. Hence Eq. (29.2) is written in terms of the principal stress differences. In the case of a uniaxial deformation $\lambda = \lambda_1$ in the 1 direction Eq. (29.2) becomes:

$$\sigma_{11} - \sigma_{22} = \lambda_1\, w'(\lambda_1) - \lambda_2\, w'(\lambda_2) \qquad (29.3)$$

and because of the incompressibility condition that $\lambda_1\lambda_2\lambda_3 = 1$ we find that $\lambda_2 = \lambda_1^{-1/2}$ and Eq. (29.3) becomes:

$$\sigma_{11} - \sigma_{22} = \lambda\, w'(\lambda) - \lambda^{-1/2} w'(\lambda^{-1/2}), \qquad (29.4)$$

where $\lambda = \lambda_1$. For uniaxial extension $\lambda > 1$ while for uniaxial compression $\lambda < 1$.

From a practical viewpoint, Eq. (29.4) can be used to describe the stress–strain relation of a material if $w'(\lambda)$ is known. $w'(\lambda)$ can be obtained in the laboratory in various ways, such as pure shear experiments as described by Valanis and Landel [60], by torsional measurements as described by Kearsley and Zapas [62] and by a combination of tension and compression experiments as also described by Kearsley and Zapas [62]. Treloar and co-workers [63] have also shown that the VL function description of the mechanical response of rubber is a very good one. The reader is referred to the original literature for these methods.

Another point to keep in mind here is that, in most models, the description of rubber elasticity given from statistical mechanical models results in a Valanis–Landel form of strain energy density function. This will be important in the following developments. We now look at some common representations of the strain energy density function used to describe the stress–strain behavior of crosslinked rubber.

There are two common phenomenological strain energy functions that have been used to describe the stress–strain response of rubber [58,59,64]. These are referred to as the Neo-Hookean form and the Mooney–Rivlin form and both can be written as Valanis–Landel forms, although they represent truncated forms of more general strain energy density functions. The Neo-Hookean form is a special form of the Mooney–Rivlin form, so we will begin with the latter. For a Mooney–Rivlin material the strain energy density function is written as:

$$W(\lambda_1,\lambda_2,\lambda_3) = C_1(\lambda_1^2 + \lambda_2^2 + \lambda_3^2 - 3) + C_2(\lambda_1^{-2} + \lambda_2^{-2} + \lambda_3^{-2} - 3) \qquad (29.5)$$

and we see that the VL function for this is of the form $w(\lambda_i) = C_1\lambda_i^2 + C_2\lambda_i^{-2}$ and the VL derivative is given as:

$$w'(\lambda_i) = 2C_1\lambda_i - 2C_2\lambda_i^{-3}, \qquad (29.6)$$

where C_1 and C_2 are material constants, often referred to as the Mooney–Rivlin Coefficients.

For uniaxial deformations of magnitude λ one then writes Eq. (29.4) for the Mooney–Rivlin stress–strain response as:

$$\sigma_{11} - \sigma_{22} = (\lambda^2 - 1/\lambda)\{2C_1 + 2C_2/\lambda\}. \qquad (29.7)$$

Equation (29.7) makes obvious the reasons for the representation of experimental data in the so-called Mooney–Rivlin plot. If the material has a Mooney–Rivlin strain energy density function then a plot of $(\sigma_{11} - \sigma_{22})/(\lambda^2 - 1/\lambda)$ vs. $1/\lambda$ results in a straight line with the slope and intercept at $\lambda = 1$ determining $2C_2$ and $(2C_1 + 2C_2)$, respectively.

For the Neo-Hookean material, the strain energy density function is the same as the Mooney–Rivlin material but with $C_2 = 0$:

$$W(\lambda_1,\lambda_2,\lambda_3) = C_1(\lambda_1^2 + \lambda_2^2 + \lambda_3^2 - 3). \qquad (29.8)$$

The VL derivative is:

$$w'(\lambda_i) = 2C_1\lambda_i. \qquad (29.9)$$

The corresponding reduced stress σ_R is:

$$\sigma_R = (\sigma_{11} - \sigma_{22})/(\lambda^2 - 1/\lambda) = 2C_1. \qquad (29.10)$$

Hence, in the Mooney–Rivlin plot, the stress–strain data are reduced to a line of slope zero.

A point worth noting here is that several of the molecular models that will be described in the subsequent sections are Neo-Hookean in form. Normally, dry rubbers do not exhibit Neo-Hookean behavior. As for the Mooney–Rivlin form of strain energy density function, rubbers may follow such behavior in extension, yet they do not behave as Mooney–Rivlin materials in compression. In Fig. 29.2, we depict typical experimental data for a polydimethylsiloxane network [39] and compare the response to Mooney–Rivlin and Neo-Hookean behaviors. The horizontal lines represent the affine and the phantom limits (see "Network Models" in Section 29.2.2). The straight line in the range $\lambda^{-1} < 1$ shows the fit of the Mooney–Rivlin equation to the experimental data points.

Statistical Theories

Structural Characteristics of Polymer Networks

In this section we discuss the most important structural parameters characteristic of an ideal polymer network. The structure of a real network always displays deviation from that of an ideal network. Network defects, such as unreacted functionalities, cyclic structures and entanglements, arise from the statistics of the crosslinking process. The crosslinking reaction, in general, results in a length distribution for the network chains. In addition to the molecular imperfections, real networks always contain inhomogeneities, i.e., regions in which the polymer concentration is permanently higher than the average concentration. The topological structure of any real network can be very complex and treatment of the topology is beyond the scope of the present work. (The reader is referred to [56,66–69] for discussions of this topic.) It is worthwhile, however, to define the structural parameters for a perfect network because it allows us to treat any real network by reference to these parameters.

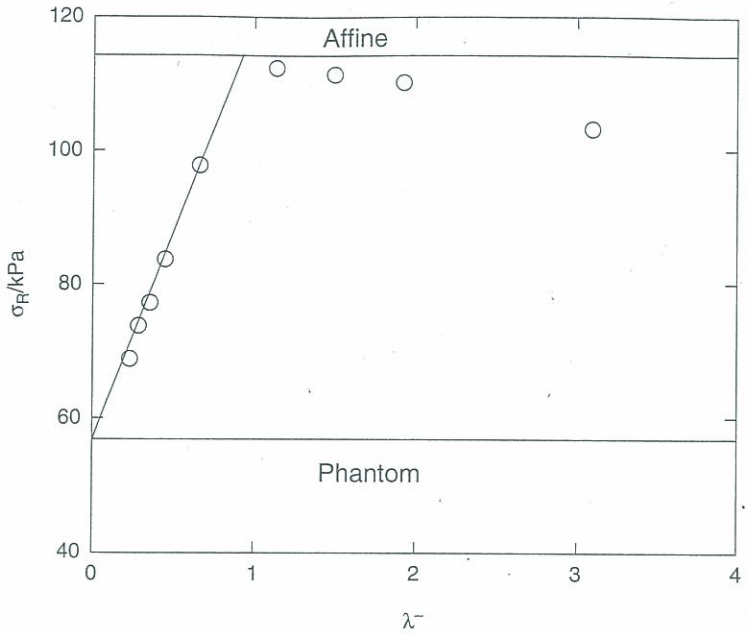

FIGURE 29.2. Comparison of typical stress–strain data for PDMS rubber [39] in a "Mooney–Rivlin" plot with "Neo-Hookean" and "Mooney–Rivlin" strain energy function descriptions. (See text for discussion).

Statistical models yield explicit expressions for the relation between the molecular structure of the network and the elastic properties.

The most important molecular parameter characteristic of a polymer network is the concentration of the elastic chains or that of the crosslinks connecting the macromolecules. An active junction is joined by at least three paths to the polymer network and an active chain is defined as one terminated by active junctions at both ends. There are several ways to express the extent of crosslinking: (1) the concentration of the elastically active chains, ν_{el}/V_0, where ν_{el} is the number of chains connecting two elastically active junctions and V_0 is the volume of the dry network, (2) the molecular weight of the polymer chains between the junctions

$$M_c = \rho(V_0 N_A/\nu_{el}), \tag{29.11}$$

where ρ is the density of the polymer and N_A is Avogadro's number, (3) the crosslink density, μ_{el}/V_0, where μ_{el} is the number of the crosslinks and (4) the cycle rank density, ξ/V_0, where ξ is the cycle rank, i.e., the number of the independent circuits in the system. Naturally, these quantities are not independent. The relationship between ν_{el}, μ_{el}, and ξ for a perfect network is given by [35]

$$\xi = \nu_{el} - \mu_{el} + 1. \tag{29.12}$$

In Fig. 29.3 a network structure is shown with $\xi = 4$, $\nu_{el} = 12$, and $\mu_{el} = 9$.

Another important parameter is the crosslink functionality, f, which is the number of chains emanating from a network junction. Only junctions with functionality higher than 2 are elastically active. For perfect networks, i.e., crosslinked polymers containing no defects, ν_{el} and μ_{el} are connected by the functionality of the crosslinks [70]

$$\mu_{el} = (2/f)\nu_{el}. \tag{29.13}$$

Real networks always contain molecular imperfections, such as pendant chains bound to the network at one end only, intramolecular loops formed by linking of two units of the same chain, and intermolecular entanglements. For an imperfect tetrafunctional network Flory [4,65] proposed a simple formula for correction for pendant chains

$$\nu_{el} = \nu_0(1 - 2M_c/M_n), \tag{29.14}$$

where ν_0 is the total number of chains in the network and M_n is the number average molecular weight of the primary molecules.

The extent to which entanglements contribute to network elasticity is not yet fully resolved. In the model of Langley[45], Dossin and Graessley [46–49] a contribution to the equilibrium modulus is associated with the plateau modulus of viscoelasticity. On the other hand, Flory [36] and Erman [38–40] assume that interpenetration of chains is solely reflected by suppression of the fluctuations of junctions.

Another type of network defect occurs due to the presence of inhomogeneities. Clustering of chains or network junctions causes permanent departures from the homogeneous distribution of the polymer throughout the gel. Regions of higher polymer concentration build up that appear as permanent departures from uniformity. They are specific to the given system and dependent upon the condition of crosslinking. The effects of inhomogeneities on the elastic and swelling behavior of the networks has not been considered

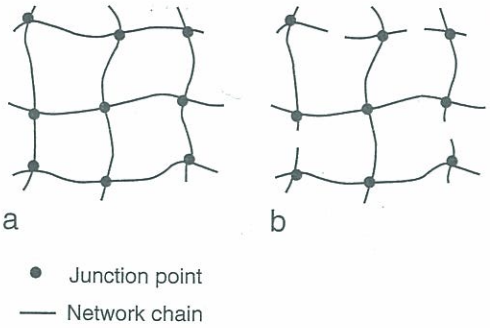

FIGURE 29.3. Schematic representation of a network structure with $\nu_{el} = 12$, $\mu_{el} = 9$, and $\xi = 4$ (a). Note that the cycle rank is the number of cuts needed to reduce the network to a tree (b).

quantitatively in any theoretical models of rubber elasticity. The reader is referred to several relevant papers in references [71–74].

Network Models

The primary goal of a general statistical theory is to derive an equation of state for the elastomeric molecular network which will hold for any deformation including swelling. Since the major contribution to the elasticity is entropic the molecular interpretation depends on how the stress affects the conformational distribution of an assembly of chains. The successful statistical model will provide predictive relationships between the molecular structure and topology of the network and its macroscopic behavior, e.g., mechanical and swelling responses.

The classical theories of rubber elasticity rest on two basic assumptions [4]:

1. The elastic free energy of the network is the sum of the elastic free energies of the network chains, i.e., the interactions between the constituent chains are independent of the state of deformation, and do not make any contribution to the elastic free energy; and
2. The end-to-end distribution of the network chains is Gaussian, i.e., the excluded volume interactions are ignored.

The affine and the phantom models derive the behavior of the network from the statistical properties of the individual molecules (single chain models). In the more advanced constrained junction fluctuation model the properties of these two classical models are bridged and interchain interactions are taken into account. We remark for completeness that other molecular models for rubber networks have been proposed [32,57,75–87], however, these are not nearly as widely used and remain the subject of much debate. Here we briefly summarize the basic concepts of the affine, phantom, constrained junction fluctuation, diffused constraint, tube and slip-tube models.

The Affine Model. In the early version of this model it was assumed that the components of length at all scales are deformed affinely [88,89], i.e., local deformations are the same as the macroscopically imposed deformation. Later this view was revised to treat only the displacement of the mean positions of the junctions and the end-to-end vectors of the chains as transforming affinely [6]. Fluctuations of the network junctions are completely suppressed by intermolecular entangling with neighboring coils sharing the same region of space. The elastic free energy of the affine network is given by [35,88–90]

$$\Delta F_{el}^{aff}/kT = (\nu_{el}/2V_0)(\lambda_1^2 + \lambda_2^2 + \lambda_3^2 - 3) - (\mu_{el}/V_0)\ln(\lambda_1\lambda_2\lambda_3), \tag{29.15}$$

where ν_{el} and μ_{el} are the number of elastic chains and junctions in the network, respectively. λ_1, λ_2, and λ_3 are the principal deformation ratios, k is the Boltzmann constant and T is absolute temperature. Here we note that the affine model is of the Neo-Hookean form with $C_1 = \nu_{el}/2V_0$, if there is no volume change upon deformation. Note also the presence of a logarithmic term in the free energy expression.

The Phantom Model. In this model polymer chains are allowed to move freely through one another and the network junctions fluctuate around their mean positions [3,91–93]. The conformation of each chain depends only on the position of its ends and is independent of the conformations of the surrounding chains with which they share the same region of space. The junctions in the network are free to fluctuate around their mean positions and the magnitude of the fluctuations is strain invariant. The positions of the junctions and of the domains of fluctuations deform affinely with macroscopic strain. The result is that the deformation of the mean positions of the end-to-end vectors is not affine in the strain. This is because it is the convolution of the distribution of the mean positions (which is affine) with the distribution of the fluctuations (which is strain invariant, i.e., nonaffine). The elastic free energy of deformation is given by

$$\Delta F_{el}^{ph}/kT = (\xi/2V_0)(\lambda_1^2 + \lambda_2^2 + \lambda_3^2 - 3) \tag{29.16}$$

and again the free energy function is of the Neo-Hookean form, with $C_1 = \xi/2V_0$.

The Constrained Junction Fluctuation Model. The affine and phantom models are two limiting cases on the network properties and real network behavior is not perfectly described by them (recall Fig. 29.2). Intermolecular entanglements and other steric constraints on the fluctuations of junctions have been postulated as contributing to the elastic free energy. One widely used model proposed to explain deviations from ideal elastic behavior is that of Ronca and Allegra [34] and Flory [36]. They introduced the assumption of constrained fluctuations and of affine deformation of fluctuation domains.

In the constrained junction fluctuation model [36,38–40] developed by Flory and Erman the spatial fluctuations of junctions are inhibited from the large values allowed in the phantom network by restrictions due to neighboring chains. The effect of conformational constraints is assumed to be imposed solely on the network junctions. The situation is illustrated by Fig. 29.4. The mean position of the network junction is located at point A. In a phantom network (Fig. 29.4(a)) the radius of the circle shows the average root-mean-square fluctuation $\langle(\Delta R)^2\rangle_{ph}^{1/2}$ around the mean position. The domain of constraints due to intermolecular interactions with neighboring chains and to steric requirements is represented by the smaller circle in Fig. 29.4(b). This latter is centered at point B. Because of the effect of constraints, the mean position of the junction (i.e., the equilibrium position in the unstrained network) is removed from point A to point C. The instantaneous position of the junction may differ significantly, however, from the equilibrium position because the junction fluctuates around its mean position. Thus, in addition to the phantom network contribution to the free energy, an important new parameter in this model is the measure of the severity of the constraints relative to those imposed by a phantom network $\kappa = <\Delta R^2>_{ph}/<\Delta s^2>_0$ where $<\Delta R^2>_{ph}$ is the mean-squared fluctuation in the positions of junctions from their mean locations in the phantom model, and $<\Delta s^2>_0$ is the mean-squared fluctuation of junctions from their mean positions under the action of constraints. The range of κ therefore is from 0 (phantom limit) to ∞ (affine limit). The size of the domains of constraints is assumed to decrease with increasing strain so that the junction fluctuations become larger. If the network is deformed the fluctuations become anisotropic in the stretching direction because the constraints become smaller.

The elastic free energy is given by

$$\Delta F_{el} = \Delta F_{el}^{ph} + \Delta F_{el}^{c} \tag{29.17}$$

where ΔF_{el}^{c} is the contribution to the elastic free energy arising from entanglement constraints relative to those in the phantom network ΔF_{el}^{ph} (see Eq. 29.16). This term can be written

$$\frac{\Delta F_{el}^{c}}{kT} = \frac{\mu_{el}}{2V_0}\sum_{t=1}^{3}[(1+g_t)B_t - \ln((B_t+1)(g_tB_t+1))] \tag{29.18a}$$

with

$$B_t = (\lambda_t - 1)(1 + \lambda_t - \zeta\lambda_t^2)(1+g_t)^{-2}, \tag{29.18b}$$

$$g_t = \lambda_t^2[\kappa^{-1} + \zeta(\lambda_t - 1)], \tag{29.18c}$$

where the parameter ζ characterizes the nonaffine transformation of the domains of constraint with deformation.

Importantly, the model spans the behavior between the phantom and affine models. When $\kappa = \infty$ and $\zeta = 0$ we recover the affine network behavior. In this case the junction fluctuations are completely suppressed, i.e., $<\Delta s^2>_0 = 0$. When $\kappa = 0$, i.e., the junctions are free to fluctuate, we recover the phantom network model.

The constrained junction fluctuation theory was modified by Erman and Monnerie [94]. The fundamental difference between the modified and the original models is the adoption of the assumption that constraints affect the centers of mass of the chains rather than the junction points only. They considered two different cases: (1) the fluctuations of all points along the chains in the phantom network are independent of macroscopic strain (constrained chain scheme, CC) and (2) the fluctuations of the points in the phantom network are dependent on the macroscopic strain, only the junctions are invariant to strain (modified constrained chain

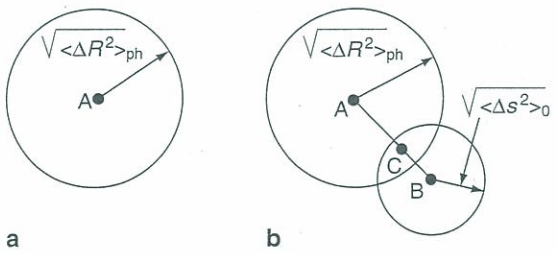

FIGURE 29.4. Effect of constraints on the fluctuations of network junctions. (a) Phantom model and (b) constrained junction fluctuation model. Note that the domain boundaries (circles in the figures) are diffuse rather than rigid. The action of domain constraint is assumed to be a Gaussian function of the distance of the junction from B similar to the action of the phantom network being a Gaussian function of ΔR from the mean position A.

scheme, MCC). The important consequence is that κ of the constrained junction fluctuation theory has been replaced by the function [94]

$$h(\lambda_x) = \kappa_G[1 + (\lambda_x^2 - 1)\Phi]^{-1}, \tag{29.19a}$$

where κ_G is a parameter corresponding to κ, and

$$\Phi = (1 - 2/f)^2/3 \quad \text{(CCmodel)}, \tag{29.19b}$$

$$\Phi = (1 - 2/f)^2 \quad \text{(MCCmodel)}. \tag{29.19c}$$

Both constrained chain models predict that the elastic modulus exceeds the value obtained from the phantom model, and according to the MCC scheme it exhibits a more sensitive dependence upon elongation or swelling than given by the original Flory–Erman theory. The effect of constraints is represented by a single parameter κ_G instead of the two parameters κ and ζ in the previous model, which makes the new theory more straightforward for the interpretation of the experimental stress–strain-swelling data.

We note that the free energy function in the Flory–Erman model is a specific form of the Valanis–Landel strain energy density function. McKenna and Hinkley [61] determined the Valanis–Landel function for the junction constraint model

$$w'(\lambda_t) = \xi kT\lambda_t + (\mu_{el}kT/2)\{B_t^*(1 + g_t) + g_t^*B_t - B_t^*(B_t + 1)^{-1} - (g_tB_t^* + B_tg_t^*)(g_tB_t + 1)^{-1}\}, \tag{29.20}$$

where

$$B_t^* = B_t\{[2\lambda_t(\lambda_t - 1)] - 1 + (1 - 2\zeta\lambda_t)[2\lambda_t(1 + \lambda_t - \zeta\lambda_t^2)]^{-1} + 2g_t^*(1 + g_t)^{-1}\} \tag{29.21}$$

and

$$g_t^* = \kappa^{-1} - \zeta(1 - 3\lambda_t/2). \tag{29.22}$$

We will come back to these models subsequently.

Diffused Constraint Model of Polymer Networks. This model, which is an extension of the Erman–Monnerie model, is more realistic in that the constraints are assumed to act continuously along the chains, instead of allowing the constraints to affect only the fluctuations of the junctions or the centers of mass of the network chains. Because the constraints affect fluctuations of all points along the macromolecule, the elastic energy of constraints must be averaged over all segments of the chain. Following a similar argument used by Flory [36] in the original constrained-junction theory, Kloczkowski, Mark, and Erman [95] derived the elastic free energy of the constraints

$$\Delta F_{el^c} = \frac{1}{2}\nu kT\sum_{t=1}^{3}\int_0^1 W(\theta)[B_t(\theta) + D_t(\theta) - \ln[B_t(\theta) + 1] - \ln[D_t(\theta) + 1]]d\theta \tag{29.23}$$

with

$$B_t(\theta) = \frac{\kappa^2(\theta)(\lambda_t^2 - 1)}{[\lambda_t^2 + \kappa(\theta)]^2} \tag{29.23a}$$

and

$$D_t(\theta) = \frac{B_t(\theta)\lambda_t^2}{\kappa(\theta)}. \tag{29.23b}$$

In Eq. (29.23) $W(\theta)$ is the distribution of constraints among different points along the network chain and $\theta = i/n$ is the position of the ith segment of the chain as a fraction of the contour length between two crosslinks. If the distribution is uniform, then $W(\theta) = 1$ inside the integrand of Eq. (29.23). In the case when constraints are assumed to affect only fluctuations of junctions (as in the constrained-junction theory), θ is limited to $\theta = 0$ or $\theta = 1$ only. [95] It is important to note that this theory does not reduce identically to the constrained-chain theory, because the latter characterizes the deformation-dependent fluctuations of the centers of mass of the chains and not the deformation-independent fluctuations of the midpoints [95].

In summary, the common feature of all constrained chain models is that they impose only limited constraints on chain fluctuations. [101] The constrained-junction fluctuation model restricts fluctuations of junctions and of the center of mass of network chains. The diffused constraint model restricts fluctuations of a single randomly chosen monomer for each network strand. Consequently, all these models can only represent the crossover between the phantom and affine limits. [101] The phantom limit corresponds to a weak constraining case, while the affine limit corresponds to a very strong constraining potential.

Tube Models. Several versions of the tube models have been developed. These models take into account the fact that constraints act along the whole chain and restrict the fluctuations of all monomers of the chain. The tube models consider that each network strand is confined within a configurational tube with a harmonic potential modeling topological constraints of entanglements. [101,120] The field is described as an uncrossable tube of constraints the centerline of which is the primitive path of the strand. The constraining field of force penalizes excursions of a strand [126] from its primitive path, i.e., a random-walk trajectory running from one network junction to the other. [126] The free energy penalty increases with excursion amplitude. The elastic free energy is given by the sum of two terms. One has the Gaussian form due to chain connectivity, while the other represents the loss of the degrees of freedom of the chains due to their spatial localization originating from entanglements. [120]

In the Edwards tube model [80] the topological potential is applied to every monomer of the chain restricting its fluctuations to a confining tube with the diameter $a \approx bN_e^{1/2}$ where N_e is the degree of polymerization between network entanglements. [101] In the model this

potential is independent of the network deformation and the tube diameter changes affinely with the macroscopic deformation of the network, $a \sim \lambda$. However, this assumption is unrealistic and disagrees with the experimental observations. [97,101]

In the Gaylord–Douglas model [57,81] the chains are localized in a tube defined by the interactions with neighboring chains. The first term of the elastic free energy is the same as that of a phantom network model, while the second term accounts for the loss of degrees of freedom of the chains due to chain localization. In the dry network the cross-sectional dimension of the tube is of the order of the hard-core cross-sectional radius of the polymer chain, and the volume of the tube is comparable with the chain molecular volume. The tube volume is considered to be invariant with macroscopic strain, since the molecular volume of the chains is independent of the deformation. The elastic free energy is given by

$$\Delta F_{\mathrm{el}} = (G_{\mathrm{net}}/2)(\lambda_1^2 + \lambda_2^2 + \lambda_3^2 - 3) + G_{\mathrm{e}}(\lambda_1 + \lambda_2 + \lambda_3 - 3), \tag{29.24}$$

where

$$G_{\mathrm{net}} = \nu_{\mathrm{el}} kT/(2V_0) \tag{29.24a}$$

and

$$G_{\mathrm{e}} = \gamma G_{\mathrm{net}} + G_{\mathrm{N}}. \tag{29.24b}$$

G_{N} is the plateau modulus of the polymer melt, V_0 is the volume of the dry network, and γ is a constant. In the absence of localization interactions, $G_{\mathrm{e}} = 0$, and Eq. (29.24) reduces to the result obtained for the phantom model. Since the constraining effect of the surrounding network chains diminishes upon swelling, G_{e} is predicted to depend on swelling as well as the conditions under which the network was formed [32,96]. The concentration dependence of G_{e} is especially large for lightly crosslinked gels (roughly linear in the concentration), however, the concentration dependence for highly crosslinked networks is relatively weak (comparable to that of the phantom model).

A challenging problem in the theory of rubber elasticity is to determine how the macroscopic deformation of the network affects the conformation of the polymer chains. At macroscopic length scales polymer networks behave as elastic solids, while at microscopic length scales the network chains move relatively freely. The elasticity is mainly entropic and is governed by deformations occurring on short length scales. Therefore, it is important to distinguish between affine and nonaffine length scales. [97] The affine length is the shortest length scale at which the network deformation is the same as that of the macroscopic deformation of the sample. At smaller length scales the deformation of the network chains is nonaffine. [97]

The nonaffine tube model developed by Rubinstein and Panyukov [97] captures the basic features of the phantom and affine models. In this model the amplitude of fluctuations that defines the tube diameter changes proportionally with the deformation of the network. The network deforms affinely on length scales larger than the affine length, R_{aff}. However, on length scales smaller than R_{aff} the confining potential has little effect on the conformation of the individual chains. The most important feature of this model is that the tube diameter a changes nonaffinely with network deformation $a \sim \lambda^{1/2}$. The prediction for the elastic free energy and the reduced force of the nonaffine tube model is [97]

$$\Delta F^{\mathrm{el}} = \Delta F^{\mathrm{el}}_{\mathrm{ph}} + \frac{ckT}{2N_{\mathrm{e}}} \sum_{\alpha} \left(\lambda_\alpha + \frac{1}{\lambda_\alpha}\right), \tag{29.25}$$

$$f^*(\lambda^{-1}) = G_{\mathrm{ph}} + \frac{G_{\mathrm{e}}}{\lambda - \lambda^{1/2} + 1}, \tag{29.26}$$

where c is the monomer concentration, G_{ph} is the phantom modulus, G_{e} is the entanglement contribution to the modulus, and N_{e} is the number of monomers between entanglements.

A more advanced version of this model combines the ideas of slip-link [98] and tube models. The "slip-tube" model allows slippage of the network chains and redistribution of the monomers between different sections of the tube [101]. The idea of slippage of the chain along the contour of the tube was originally proposed by de Gennes [105] in the reptation model of polymer melts, and the analysis of the redistribution of stored length was made by Doi [100]. The basic concept of the slip-link models is that permanent entanglements act as slip-links connecting neighboring chains. The slip-links are allowed to pass through each other, but each of them can slide along the chain only up to a limited distance. [101] If this distance is equal to the chain length, the slip-link model reduces to the phantom network model. In the opposite limit, when the sliding distance of the slip-links is small compared to the average distance between neighboring slip-links, the model is reduced to the affine model.

In the slip-tube model [101] the topological constraints imposed by the neighboring network chains are represented by virtual chains attached to the elastic nonfluctuating background at one end and ending with slip-links at the other. The network chains pass through these slip-links but they are not allowed to pass through each other. [101] The amplitude of the slip-link fluctuations depends on the density of the slip-links. At high density the slip-links are located at every monomer and the fluctuations are completely suppressed. In this limit the slip-tube model reduces to the nonaffine tube model. If slippage along the tube is allowed the network chains redistribute their lengths along the contour of their confining tubes. [101] In the anisotropically deformed network the number of monomers in a given direction α will be changed due to the slippage.

The elastic free energy of the network is given as [101]

$$\Delta F^{el} = \Delta F^{el}_{ph} + \frac{kT\nu L}{2}\sum_{\alpha}\left(\frac{\lambda_\alpha}{g_\alpha^{1/2}} + \frac{g_\alpha^{1/2}}{\lambda_\alpha}\right) - \nu TS\{g_\alpha\}, \tag{29.27}$$

where L is the number of slip-links per network chain and g_α is the "redistribution parameter" that depends on the number of monomers along the axis α in the deformed network relative to that in the undeformed network. The function $S\{g_\alpha\}$ is related to the entropy of the degrees of freedom corresponding to different positions of slip-links along the chains.

Numerical solution of the slip-tube model yields for the reduced stress [101]

$$f^*(\lambda^{-1}) = G_{ph} + \frac{G_e}{0.74\lambda + 0.61\lambda^{1/2} - 0.35}. \tag{29.28}$$

In this equation the deformation ratio λ appears only in the entanglement contribution. Thus, the experimental data can be analyzed in the form of a universal plot. Moreover, Eq. (29.28) allows one to separate the phantom and entanglement contributions to the elasticity of the network.

The Mixing Contribution to the Free Energy

So far we have discussed the behavior of networks in the dry state. In the case of a swollen network additional effects must be taken into account. The thermodynamics of mixing is governed by the interaction between the polymer and the solvent molecules. As we have seen in "Network Models" in Section 29.2.2 in gels the fluctuations of the network junctions are significantly altered by the presence of crosslinks. The formulation of a mixing free energy for the swollen network would require the detailed knowledge of the effect of osmotic forces on the size and shape of the fluctuation domains. This is beyond the scope of the existing molecular theories.

Because of the lack of an explicit molecular theory which accounts for the effect of crosslinking on the structure of a polymer solution, it is generally assumed that the functional dependence of the free energy of mixing in the swollen network is the same as in a polymer solution. Although this is a strong approximation, the application of the theoretical free energy functions derived for polymer solutions provides a simple and straightforward way to interpret the results of mechanical and swelling measurements performed on swollen polymer networks. There are two essentially different ways to describe the thermodynamics of polymer solutions: classical (mean field) theories [4] including recent renormalized models [102,103] and asymptotic scaling theories [104,105] based on the analogy found between critical phenomena and polymer chain statistics.

Flory–Huggins Theory of Polymer Solutions

The classical treatment of polymer solution thermodynamics due to Flory and Huggins [4] is based on a lattice model which assumes a uniform polymer segment concentration throughout the entire system. The free energy of mixing of a polymer solution is given by

$$\Delta F_{mix} = RT[n_1 \ln(1-\varphi) + n_2 \ln\varphi + \chi n_1\varphi)], \tag{29.29}$$

where φ is the volume fraction of the polymer, χ is the Flory–Huggins interaction parameter, and n_1 and n_2 are the numbers of moles of solvent and polymer, respectively. The chemical potential of the solvent is defined as the derivative of the free energy of mixing with respect to amount of solvent

$$(\Delta\mu_1)_{mix} = (\partial\Delta F_{mix}/\partial n_1) = RT[\ln(1-\varphi) + (1-N^{-1})\varphi + \chi\varphi^2], \tag{29.30}$$

where N is the degree of polymerization. For a crosslinked polymer $N = \infty$. In general, χ depends on the polymer concentration [106], i.e.,

$$\chi = \chi_0 + \chi_1\varphi + \ldots, \tag{29.30a}$$

where χ_0 and χ_1 are constants.

Scaling Theory

In the 1970s a new theory of polymers, taking account of correlations between monomers, was developed based on the analogy found between polymer statistics and critical phenomena [105]. For the chemical potential of mixing in the semidilute region scaling theory yields

$$(\Delta\mu_1)_{mix} = ART\varphi^n \quad (\varphi^* < \varphi \ll 1), \tag{29.31}$$

where the prefactor A is characteristic of the polymer/solvent system and the value of the exponent n depends on the thermodynamic quality of the solvent. In a good solvent $n \approx 2.31$, and in the theta condition n=3. φ^* is the polymer volume fraction above which the domains of the coils start to overlap, i.e., the volume fraction of the polymer inside a separate coil

$$\varphi^* \propto N/R^3 \propto N^{1-3\nu}, \tag{29.32}$$

where ν is the excluded volume exponent, the value of which is $\nu \approx 3/5$ (good solvent condition) or $\nu = 1/2$ (theta condition).

De Gennes proposed a description of the properties of swollen polymer networks based on the analogy found between the swollen network and semidilute polymer solutions (φ^* theorem) [105]. The fully swollen gel is expected to maintain a polymer volume fraction, φ_e, which is proportional to the overlap concentration. In good solvent condition

$$\varphi_e = z(f)\varphi^* \propto z(f)(1/2-\chi)^{-3/5}N^{-4/5}, \tag{29.33}$$

where $z(f)$ is a constant factor of the order of unity and f is the crosslink functionality.

Many attempts to explain the results of osmotic and mechanical measurements on swollen polymer networks have invoked analogies with semidilute polymer solutions. Scaling forms for different physical quantities have been derived from the φ^* theorem.

For example, the elastic (shear) modulus of a gel is given by [99,105]

$$G = B(\varphi_e/N_c), \tag{29.34}$$

where φ_e is the volume fraction of the polymer in the fully swollen gel, N_c is the degree of polymerization between crosslink points and B is a constant which depends on the polymer/solvent system. From Eqs. (29.32) and (29.34) it follows that

$$G = B\varphi_e^n, \tag{29.35}$$

where $n = 3\nu/(3\nu - 1)$. Equation (29.35) predicts that the concentration dependence of the elastic moduli of gel homologues (chemically similar gels having different crosslinking densities) follows a simple power law behavior. The value of n depends on the thermodynamic quality of the solvent: in good solvent condition $n \approx 2.31$, in theta condition n=3.

Here we note that in the simple scaling theory used earlier, the polymer is considered as an infinitely thin chain possessing length but not volume. At higher polymer concentration, however, the finite volume of the structural elements may no longer be neglected. Advanced scaling theories [102,103] using the Flory–Huggins lattice model as a starting point are able to incorporate the polymer volume into their formalism.

Swelling of Polymer Networks—The Frenkel–Flory–Rehner Hypothesis

A crosslinked polymer exposed to a thermodynamically compatible diluent absorbs solvent molecules. The driving force of the mixing process is mainly entropic. As the volume increases the network chains are deformed and an elastic retractive force develops. The chain deformation causes a decrease in the entropy, because the extended configuration of the chains is less probable. Equilibrium is achieved when these opposing forces are balanced.

The basic assumption in the Frenkel–Flory–Rehner theory describing the swelling of a crosslinked polymer is that the elastic (ΔF_{el}) and mixing (ΔF_{mix}) contributions in the free energy that accompanies the swelling of the dry network are separable and additive [2,4,5]

$$\Delta F = \Delta F_{el} + \Delta F_{mix}, \tag{29.36}$$

where ΔF is the total free energy of the polymer–solvent system. At equilibrium with the pure solvent (at constant temperature and pressure) the free energy is at minimum with respect to any changes in composition, i.e.,

$$\begin{aligned}(\partial \Delta F/\partial n_1) &= \mu_1 - \mu_1^0 = 0 \\ &= (\mu_1 - \mu_1^0)_{mix} + (\mu_1 - \mu_1^0)_{el},\end{aligned} \tag{29.37}$$

where n_1 is the number of moles of solvent, μ_1 is the chemical potential of solvent in the gel and μ_1^0 is the chemical potential of the pure solvent. The subscripts mix and el refer to the mixing and elastic contributions to the chemical potential, respectively. How the Frankel–Flory–Rehner model can be used to relate macroscopic swelling observations to the molecular structure of the network is developed subsequently.

Experimental Characterization of Swollen Polymer Networks

Molecular theories of rubber elasticity (see "Network Models" in Section 29.2.2) allow the interpretation of the experimental data obtained for elastomeric materials in terms of structural characteristics of the network. The most frequently used experimental techniques are stress–strain measurements and swelling measurements.

Stress–Strain Isotherms

Uniaxial stress–strain measurements are often used to characterize polymer networks both in the dry state and in equilibrium with a diluent. The analysis of the stress–strain isotherms is usually performed in terms of the reduced force

$$[f^*] = f^*\varphi^{1/3}/(\alpha - \alpha^{-2}), \tag{29.38}$$

where f^* is the force per unit unstrained cross-section of the unswollen network and α is the deformation ratio relative to the undeformed swollen state of volume V. The relationship between α and λ is given by

$$\lambda_1 = \alpha(V/V_0)^{1/3} \tag{29.39a}$$

and

$$\lambda_2 = \lambda_3 = \alpha^{-1/2}(V/V_0)^{1/3}. \tag{29.39b}$$

In both the phantom and affine models the reduced force is identified with the elastic modulus. In the affine limit the shear modulus is expressed as

$$G_{aff} = [f^*]_{aff} = kT(\nu_{el}/V_0), \tag{29.40}$$

while in the phantom limit

$$G_{ph} = [f^*]_{ph} = kT(\xi/V_0). \tag{29.41}$$

In general, experimental stress–strain isotherms differ from the predictions of the simple statistical theories.

The constrained junction fluctuation theory provides a description of the network behavior which lies between the

affine and phantom limits [36,38–40]. According to this theory the elastic force, f, is the sum of two contributions

$$f = f_{ph} + f_c, \tag{29.42}$$

where f_{ph} is the phantom network contribution and f_c arises from the entanglement constraints. The reduced stress $[f^*]$ is given by

$$[f^*] = kT(\xi/V_0)(1 + f_c/f_{ph}) \tag{29.43}$$

and the expression for f_c/f_{ph} in uniaxial deformations is

$$f_c/f_{ph} = (\mu/\xi)[\alpha K(\lambda_x^2) - \alpha^{-2}K(\lambda_y^2)](\alpha - \alpha^{-2})^{-1}, \tag{29.44}$$

where $\lambda_1 = \lambda$ and $\lambda_2 = \lambda^{-1/2}$. The function K is defined by

$$K(\lambda_t^2) = B_t[B_t^*(B_t + 1)^{-1} + g_t(g_t B_t^* + g_t^* B_t)(g_t B_t + 1)^{-1}], \tag{29.45}$$

where B_t, B_t^* and g_t are the same as in Eqs. (29.18), (29.21) and (29.22).

The ratio f_c/f_{ph} is expected to decrease with increasing deformation, and at $\alpha^{-1} = 0$ the modulus approaches the phantom limit.

The Flory theory considers topological interactions among junctions and chains only in that they restrict junction fluctuations. Ferry [107], Langley [45], Dossin [46] and Graessley [49] assume that these interactions are also present in the small-strain limit. Their argument is based on the existence of a rubbery plateau modulus, G_N^0, which is observed in the viscoelastic properties of high molecular weight linear polymers. The plateau modulus is assumed to be a measure of the entanglement interactions between the chains. In a permanent network the interchain entanglements are fixed due to the presence of the chemical bonds. Dossin and Graessley [46] proposed that

$$G = \nu kT(1 - 2h/f)(V/V_0)^{2/3}/V + T_e G_e^{max}, \tag{29.46}$$

where G is the small-strain modulus, T_e is the fraction of the maximum concentration of topological interactions which are permanently trapped by the network, G_e^{max} is the maximum possible contribution of entangled chains to the modulus, and h is an empirical constant, the value of which is between 0 and 1, depending on the extent to which the junction fluctuations are impeded in the network (h=0 in the affine limit and h=1 in the phantom limit). Thus Eq. (29.46) predicts a small-strain modulus greater than that predicted by the Flory–Erman theory and greater than that of the affine model.

The apparent discrepancy between the Flory theory and the entanglement concept of Dossin and Graessley has been addressed by Gottlieb and Macosco [55]. They pointed out that the two parameters h and κ, both measuring the severity of constraints are related. For the case of a perfect, incompressible, unswollen network the analytical relationship is given by

$$h = 1 - (\kappa^2 + 1)(\kappa + 1 - p/2)^2(\kappa + 1)^{-4}, \tag{29.47}$$

where p is a constant. For the case of the Flory theory p=2. Importantly the Flory–Erman theory has been developed for finite (large) deformations, which is not true of the trapped entanglement model, which resultingly limits the latter's usefulness in terms of making quantitative estimates of experimental results, particularly in large deformation experiments, including swelling.

Swelling Measurements

In addition to mechanical measurements, swelling measurements are frequently used to characterize rubber networks. Of particular interest is the relationship between the molecular weight between crosslinks and the degree of swelling. Unfortunately, the numerical values of the molecular parameters obtained by elastic and swelling measurements strongly depend upon the particular theoretical model used to evaluate the experiments. The model behaviors are described in the following paragraphs. The swelling equation for a phantom network is given as [44,108]:

$$\ln(1 - \varphi_e) + \varphi_e + \chi\varphi_e^2 = -(\xi/N_A V_0)V_1\varphi_e^{1/3}, \tag{29.48}$$

while for an affine network

$$\ln(1 - \varphi_e) + \varphi_e + \chi\varphi_e^2 = -(\xi/N_A V_0)V_1\varphi_e^{1/3}[1 + (\mu/\xi)(1 - \varphi_e^{2/3})], \tag{29.49}$$

where N_A is Avogadro's number and the complexity in Eq. (29.49) arises due to the logarithmic contribution to the free energy in the affine network model (see Eqs. (29.1) and (29.15)).

The corresponding equation according to the Flory–Erman constrained junction fluctuation model is

$$\ln(1 - \varphi_e) + \varphi_e + \chi\varphi_e^2 = -(\xi/N_A V_0)V_1\varphi_e^{1/3}[1 + K(\lambda^2)], \tag{29.50}$$

where $K(\lambda^2)$ was defined previously (see Eq. (29.45)). Queslel *et al.* [108] made a comparison between the values of the molecular network parameters calculated through Eqs. (29.48)–(29.50). The highest value of M_c (chain molecular weight) is obtained by the affine model. The phantom model yields lower M_c than the affine model, because in the former junction fluctuations decrease the impact of chain entropy changes. Using Eq. (29.49) the same elastic contribution as that of an affine network is thus achieved if ξ is higher (or correspondingly M_c is smaller). The value of M_c determined from the Flory–Erman model lies between these limiting values. It is worth mentioning that Eqs. (29.48) and (29.49) enable one to estimate a range for M_c without any prior knowledge of the network structure.

Both the affine and the phantom network models predict that the reduced stress, $[f^*]$, measured in uniaxial deformation is independent of the deformation ratio. However, it

became clear from early studies of rubber elasticity that real networks, in general, exhibit significant departures from this prediction: the reduced stress decreases with elongation and also with increasing swelling. It was recognized that the limiting value of the reduced stress at high elongation or swelling ratio is a characteristic quantity of the network.

The detailed calculations according to the constrained junction fluctuation model and other advanced models can only be performed numerically. The fitting of the stress–strain (or swelling) data to the Flory–Erman model, in principle, requires three parameters: $[f^*]_{ph}$, κ and ζ. Here we briefly outline the steps of the fitting procedure [113,114]:

1. In many cases it is reasonable to take the initial value of $[f^*]_{ph} = 2C_1$, where $2C_1$ is the first Mooney–Rivlin constant. An alternative possibility is to estimate $[f^*]_{ph}$ from the stoichiometry of the chemical reaction using Eqs. (29.12)–(29.14) and (29.41).

2. The initial value of κ can be obtained from the Flory–Erman theory on the basis of the following argument [109]. Since κ is assumed to be proportional to the number of chains sharing the volume occupied by one chain, it is the measure of the degree of interpenetration of the network chains, i.e.,

$$\kappa = I<r^2>_0^{3/2}(\nu/V_0), \tag{29.51}$$

where $<r^2>_0$ is the unperturbed dimension of a chain and I is a proportionality constant. Expressing Eq. (29.51) in terms of measurable quantities one gets [109]

$$\kappa = A(2C_1)^{-1/2}\varphi_c^{(4/3)+m}, \tag{29.52}$$

where φ_c is the volume fraction of the polymer at crosslinking and
$A = I(<r^2>_{0/M})^{3/2}(1 - 2/f)N_A^{3/2}\rho^{3/2}/(kT)^{1/2}$, where N_A is Avogadro's number, ρ is the density of the polymer and f is the crosslink functionality. The experimental value of A is the order of unity (for PDMS networks Erman and Mark [110] reported A=1.29 and m=0.385).

3. In a first approximation the parameter ζ can be assumed to be zero.

4. Using these initial values the differences between theory and experiment should be minimized. In order to achieve this the value of κ obtained in step (2) is used to calculate $[f^*]_{ph}$ from Eqs. (29.43) and (29.44). Then $2C_1$ in Eq. (29.52) is replaced by $[f^*]_{ph}$ to obtain a new value of κ. These steps are iterated until κ converges. Using the new values of $[f^*]_{ph}$ and κ the function $[f^*]$ vs. α^{-1} is calculated from Eq. (29.43).

5. The procedure described in 4 is repeated for a new value of m (and A), and the values of $[f^*]_{ph}$ and κ are recalculated. The calculation is continued until the error between the experimental and the calculated data reaches a minimum.

6. If the agreement between calculated data and experiment is still not satisfactory, the value of ζ can be varied to match theory and experiment. The values of ζ giving the best agreement with experiments are usually close to zero.

29.3 ANALYSIS OF EXPERIMENTAL RESULTS

29.3.1 General Comments

The primary goal of the molecular theories is to derive the structure–property relationships for polymeric networks. A quantitative understanding of the dependence of the physical properties upon the network structure is essential to deduce molecular parameters (e.g., molecular weight between crosslinks) from measurements. This is also required to synthesize new polymer networks having desired physical properties.

To test the validity of different network theories is particularly difficult because the structure of the network, at the molecular level, is unknown. Usually crosslinks are introduced in a less perfectly controlled manner than desired. The extent of imperfections depends on the mechanism of the crosslinking process, e.g., clustering of chains or junctions may lead to deviations from the complete randomness assumed in the theories. In many cases, the distribution of the network chains and junctions is not uniform throughout the sample.

Analysis of the experimental data obtained for model networks having known structure provides a straightforward way of understanding the structure–property relationships. Such model networks can be synthesized by specific chemical reactions, e.g., by end-linking of well-characterized polymer chains through a controlled chemical reaction. The characteristics of the chains, prior to crosslinking, can be determined using the usual solution characterization techniques (gel chromatography, viscometry, etc.). In this way the average molecular weight between crosslinks (M_c) and the distribution of M_c can be varied in a controlled manner. The crosslink functionality (f) is known from the chemistry of the crosslinking reaction. Since ν_{el} and f are known. $\xi = \nu_{el} - \mu_{el} + 1$ is also known. Assuming that the chemical reaction between the endgroups of the chains and the crosslinking agent is stoichiometric, and that the effects of entanglements and network imperfections (cycles, pendent chains) are negligible, the elastic properties of the gel can be predicted. Equations (29.40) and (29.41) allow the elastic modulus both in the phantom and the affine limits to be calculated. The decrease of the modulus with λ depends on the values of κ and ζ in the Flory–Erman theory. Unfortunately, this theory does not make an a priori prediction for these parameters. Since no independent information is available about the actual size of fluctuation domains of junctions and about the anisotropy of these domains, the values of κ and ζ can only be determined empirically using a fitting procedure such as that described in "Swelling Measurements" in Section 29.2.2

The testing of the network models with regard to the prediction of the equilibrium swelling degree of the crosslinked polymer as a function of the thermodynamic activity of the diluent requires further assumptions concerning the mixing free energy contribution. This term is supposed, firstly, to be separable from the total change in the free energy (see Eq. 29.36) and, secondly, to be identical for the gel and for the solution of the uncrosslinked polymer of infinite molecular weight. The latter assumption presumes that the polymer solvent interaction parameter is unaffected by the presence of crosslinks. Thus, the only difference between the swollen network and the polymer solution is the existence of a permanent elastic modulus and the theoretical dependence of the equilibrium volume fraction upon the molecular parameters is predicted by Eqs. (29.48)–(29.50).

The structure of any real network exhibits departures from that of the ideal (model) network. A comparison between the experimental and theoretical values of the network parameters provides quantitative information on the deviation from the behavior of the hypothetical model system, and allows one to treat real networks by reference to the structural parameters of a perfect network.

In the following sections typical experimental results obtained for different network systems and analyzed using several of the theoretical approaches are briefly reviewed. For a more extensive discussion, we refer the reader to a work by Han, Horkay, and McKenna [111] where a critical evaluation of many of the modern theories of molecular rubber elasticity was performed. Based on an analysis of carefully selected data sets reported in the literature, these authors concluded that, of the tested models, the Flory–Erman theory and its modified versions provided the best agreement with the stress–strain data in both the dry and the swollen states for polymer networks.

29.3.2 Determination of the Model Parameters from Stress–Strain Measurements

A large amount of experimental work has been reported on the stress–strain behavior of swollen polymeric networks. Fitting of stress–strain data measured at different degrees of dilution to Eqs. (29.43)–(29.45) enables one to determine ξ,κ, and ζ.

Erman and Flory [39] reanalyzed the data of Allen *et al.* [112] on swollen natural rubber samples crosslinked with dicumyl peroxide. It was found that the shape of the $[f^*]$ vs. α^{-1} curves in a wide range of dilution in *n*-decane ($0.24<\varphi<1$) can be well reproduced using a single set of parameters $[f^*]_{ph} = 0.166\,\mathrm{Nmm^2}$, $\kappa = 8$, and $\zeta = 0.12$. Similar analysis of the data of Flory and Tatara [33] for radiation crosslinked PDMS samples swollen in benzene yields the values $[f^*]_{ph} = 0.136\,\mathrm{MPa}$, $\kappa = 6$, and $\zeta = 0.12$. For poly(ethyl acrylate) networks [37] having different crosslink densities swollen in bis(2-ethoxyethyl)ether κ varied in the range 1.8–16.0, and ζ varied between 0.0 and 0.1. It was also found that the stress–strain isotherms for the same networks in the unswollen state and in swelling equilibrium with a diluent are consistently described by the same set of parameters, κ and ζ. Typical $[f^*]$ vs. α^{-1} data set along with the fit of the Flory–Erman theory is shown in Fig. 29.5.

Swelling equilibrium measurements provide an independent route to determine $[f^*]_{ph}$. At swelling equilibrium the sum of the contributions to the chemical potential from

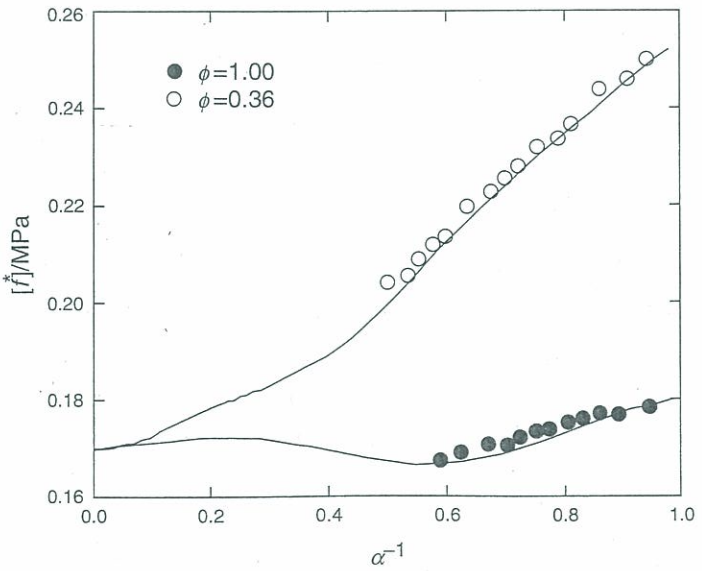

FIGURE 29.5. "Mooney–Rivlin" reduced stress plot showing comparison of experimental data with modified constrained chain model (MCC) predictions for dry (○) and swollen (●) natural rubber networks [112, 117]. Swelling agent: *n*-Decane. continuous lines are theoretical curves calculated with paremeters $\xi kT/V_0 = 0.17\,\mathrm{MPa}$ and $\kappa_G = 2.0$.

mixing and from the elastic deformation of the network should be zero (see Eq. 29.37). Thus

$$0 = \ln(1-\varphi) + \varphi + \chi\varphi^2 + (V_1\xi/N_A V_0)\lambda^{-1}[1 + K(\lambda^2)], \quad (29.53)$$

where N_A is the Avogadro number. Substitution for ξ/V_0 according to Eq. (29.41) yields

$$[f^*]_{ph} = -(RT/V_1)[\ln(1-\varphi) + \varphi + \chi\varphi^2]\lambda/[1 + K(\lambda^2)], \quad (29.54)$$

where $K(\lambda^2)$ is defined by Eq. (29.45).

Using Eq. (29.54) Erman and Flory [39] analyzed the results of Mark and Sullivan [113] on end-linked PDMS networks swollen in benzene as well as the data from Erman, Wagner, and Flory [37] on poly(ethyl acrylate). They compared the values of $[f^*]_{ph}$ obtained from stress–strain isotherms and swelling measurements with data calculated from the chemistry of crosslinking. The $[f^*]_{ph}$ values derived from elasticity measurements were slightly higher than those calculated from the known molecular weights of the primary chains on the basis of stoichiometry. The deviation was attributed to possible departures from equilibrium in the force measurements. The most pronounced departure was observed for networks of low degrees of crosslinking in which the approach of equilibrium is protracted. No such deviation was detected for $[f^*]_{ph}$ obtained from swelling measurements. The satisfactory agreement between the experimental and the calculated values of $[f^*]_{ph}$ led the authors to the conclusion that trapped entanglements do not have a significant contribution to the elastic response of the network. If the effective degree of interlinking is enhanced by discrete entanglements, the values of $[f^*]_{ph}$ deduced from elastic or swelling measurements should exceed the chemical values of $kT\xi/V_0$ calculated from the chemistry of crosslinking.

Gottlieb *et al.* [54] reached the opposite conclusion by the analysis of data on PDMS from different sources, including the same data set of Mark and Sullivan [113]. They argue that trapped entanglements contribute substantially to the stress. Erman and Flory [39] criticized this interpretation on several grounds. Their main criticism was that Gottlieb *et al.* [54] confined their attention to stresses at small strains and did not deduct the contribution to the reduced stress from restraints on junction fluctuations. In the analysis of Gottlieb *et al.* such fluctuations are assumed to be totally suppressed at small strains, as if $\kappa = \infty$ for all networks, and the contribution arising from the constraints is treated as a constant fraction of the reduced stress. This procedure may enhance the reduced forces by factors that increase with decreasing crosslink density, and lead to a finite value of $[f^*]_{ph}$ at $\xi = 0$. According to Flory and Erman [39] the large entanglement contribution in the analysis conducted by Gottlieb *et al.* [54] is largely a fiction of their data treatment.

A comprehensive analysis of previously reported stress–strain data for five different elastomers both in the swollen and unswollen states was performed on the basis of the Flory–Erman theory by Brotzman and Mark [114] (Table 29.1). They found that, in most cases, as the polymer volume fraction decreases, the value of κ required to describe the experimental data also decreases. The analysis also revealed that when ζ is set to zero the high-extension intercept of the $[f^*]_{ph}$ vs. α^{-1} curves is practically independent of the degree of swelling. In Table 29.2 the values of $2C_1$ and $2C_1 + 2C_2$ obtained for the same networks by using the linear Mooney–Rivlin equation of the reduced force, $[f^*] = 2C_1 + 2C_2\alpha^{-1}$, are listed. The $2C_1$ values are in reasonable agreement with the $[f^*]_{ph}$ data given in Table 29.1, indicating that the Mooney–Rivlin treatment can yield similar estimates of the cycle rank of the network as does the more detailed theoretical approach. Poorer agreement was found between $[f^*]_{ph}$ and $2C_1$ by Sharaf and Mark [115]. These authors re-examined the small-strain modulus data reported for unswollen PDMS model networks (Table 29.3). The values $[f^*]_{ph}$ were found two- or threefold lower than the corresponding values of $2C_1$. For comparison in Table 29.4 the characteristic quantities of the same PDMS model networks are given in terms of the entanglement model (see Eq. (29.46)).

Fontaine *et al.* [116,117] compared the prediction of the constrained chain models with the results of elongation measurements performed on dry and swollen natural rubber, poly(ethylene oxide), polybutadiene, poly(dimethylsiloxane) and *cis*-1,4-polyisoprene networks. In Table 29.5 the parameters obtained by analysis of the same network systems using both the CC and the MCC models are listed. It was found that the strong dependence of the reduced force on extension and swelling, observed in all the experiments, can be satisfactorily described by the constrained chain models. The value of the parameter, κ_G, varies between 0.9 and 6.0 for all five network systems investigated. (The other parameter, $\xi kT/V_0$, required to describe the strain and swelling dependence of the data is obtained directly from the experimental stress–strain isotherms at $\alpha^{-1} = 0$.) In the framework of the Flory–Erman model quantitative agreement between the theory and the data for the polybutadiene and poly(ethylene oxide) networks has been achieved only when both κ and the phantom modulus $\xi kT/V_0$ were allowed to be dependent on φ. The formulation according to the constrained chain models, however, does not require φ dependent values of $\xi kT/V_0$ and κ_G.

Kloczkowski, Mark, and Erman [95] compared the prediction of the diffused constraint model with the results of the Flory constrained-junction fluctuation theory [36] and the Erman–Monnerie constrained chain theory [94]. They found that the shapes of the $[f^*]$ vs. α^{-1} curves for all three theories were very similar. Rubinstein and Panyukov [101] reanalyzed the data of Pak and Flory [118] obtained for uniaxially deformed crosslinked PDMS samples. They concluded that the fit of the experimental data by the diffused

TABLE 29.1. *Parameters of the stress–strain isotherms calculated from the fit of the Flory–Erman model for different networks systems [114].*

Polymer[a]	Diluent	f	Crosslinker	T (°C)	φ	$[f^*]_{ph}$ (MPa)	κ	ζ
PDMS [134]	Lin. PDMS	4	γ-Irradiation	30	1.00	0.0325	7.66	0.00
					0.80	0.0317	4.79	0.00
					0.60	0.0317	4.10	0.00
					0.40	0.0318	3.96	0.00
					1.00	0.0355	6.75	0.05
					0.80	0.0334	4.91	0.05
					0.60	0.0330	5.02	0.05
					0.40	0.0333	4.69	0.05
					1.00	0.0366	6.94	0.10
					0.80	0.0341	6.09	0.10
					0.60	0.0335	7.72	0.10
					0.40	0.0343	9.96	0.10
PDMS [134]	Lin. PDMS	4	γ-Irradiation	30	1.00	0.0245	14.3	0.00
					0.80	0.0238	4.74	0.00
					0.60	0.0232	4.63	0.00
					0.40	0.0221	4.35	0.00
PDMS [134]	Lin. PDMS	4	γ-Irradiation	30	1.00	0.0146	15.3	0.00
					0.80	0.0139	8.23	0.00
					0.60	0.0129	10.8	0.00
					0.40	0.0130	4.77	0.00
PBD-S [135]	1,2,4-Trichlorobenzene	4	1% Sulfur	25	1.00	0.222	7.93	0.00
					0.80	0.213	6.43	0.00
					0.60	0.204	6.74	0.00
					0.40	0.192	8.07	0.00
					0.20	0.212	5.21	0.00
					1.00	0.245	6.83	0.05
					0.80	0.232	6.04	0.05
					0.60	0.227	5.47	0.05
					0.40	0.219	7.68	0.05
					0.20	0.231	12.0	0.05
					1.00	0.250	10.3	0.10
					0.80	0.237	7.77	0.10
					0.60	0.232	8.12	0.10
					0.40	0.229	25.0	0.10
					0.20	0.240	4.81	0.10
PBD-G [135]	1,2,4-Trichlorobenzene	4	γ-Irradiation	10	1.00	0.107	20.2	0.00
					0.80	0.097	16.4	0.00
					0.60	0.98	9.77	0.00
					0.40	0.93	8.11	0.00
					0.20	0.93	6.78	0.00
		24		10	1.00	0.162	24	0.00
					0.80	0.135	20	0.00
					0.60	0.127	22.8	0.00
					0.40	0.111	27.2	0.00
					0.20	0.101	29.7	0.00
PBDG-P [135]	1,2,4-Trichlorobenzene	4	1% BPO	10	1.00	0.147	2.96	0.00
					0.80	0.143	2.16	0.00
					0.60	0.142	1.42	0.00
					0.40	0.142	0.84	0.00
					0.20	0.140	1.07	0.00
		24		10	1.00	0.164	18.2	0.00
					0.80	0.153	16.1	0.00
					0.60	0.143	17.7	0.00
					0.40	0.138	25.4	0.00
					0.20	0.136	23.0	0.00

TABLE 29.1. *Continued.*

Polymer[a]	Diluent	f	Crosslinker	T (°C)	φ	$[f^*]_{ph}$ (MPa)	κ	ζ
PIB [136]	1,2,4-Trichlorobenzene	4	Disulfide	30	1.00	0.082	10.0	0.00
					0.80	0.083	2.44	0.00
					0.60	0.073	3.98	0.00
					0.40	0.070	2.65	0.00
				20	1.00	0.166	3.22	0.00
					0.80	0.104	3.74	0.00
					0.60	0.104	2.75	0.00
					0.40	0.095	3.14	0.00
				15	1.00	0.131	3.95	0.00
					0.80	0.123	4.11	0.00
					0.60	0.119	2.16	0.00
					0.40	0.107	1.21	0.00
POE [137]	Phenylacetate	3	Triisocyanate	25	1.00	0.721	1.14	0.00
					0.597	0.637	1.58	0.00
					0.565	0.549	2.26	0.00
					0.488	0.337	14.8	0.00
					0.390	0.608	1.58	0.00
POE [137]	Phenylacetate	3	Triisocyanate	25	0.429	0.608	1.56	0.00
					0.325	0.240	2.52	0.00
					0.220	0.259	0.960	0.00
POE [137]	Phenylacetate	3	Triisocyanate	25	0.457	0.314	1.29	0.00
					0.341	0.345	1.19	0.00
					0.291	0.314	1.29	0.00
					0.488	0.337	14.8	0.00
					0.390	0.608	1.58	0.00
POP [138]	Benzene		Tris(*p*-phenylisocyanate)	60	0.216	0.285	2.0	0.00
					0.216	0.315	2.2	0.00
			$M_c = 3{,}000$		0.286	0.400	1.5	0.00
			$M_c = 2{,}000$		0.286	0.417	1.7	0.00
					0.273	0.376	1.7	0.00
			$M_c = 1{,}025$		0.406	0.805	0.5	0.00
					0.421	0.773	0.5	0.00
			$M_c = 725$		0.464	0.750	0.5	0.00
					0.456	0.769	0.5	0.00
			$M_c = 730$		0.473	0.725	0.4	0.00
					0.477	0.758	0.4	0.00
					0.440	0.755	0.4	0.00
			$M_c = 740$		0.522	0.695	0.5	0.00
					0.519	0.645	0.4	0.00
			$M_c = 725$		0.480	0.850	0.5	0.00
					0.510	0.829	0.4	0.00

[a]PDMS: poly(dimethylsiloxane); PDB: *cis*-1,4-polybutadiene; PIB: polyisobutylene; POE: poly(oxyethylene); POP: poly(oxypropylene).

constraint model was significantly better than by the Mooney–Rivlin expression or by the nonaffine tube model [97].

Urayama *et al.* [119–121] tested the diffused constraint model using both uniaxial compression and equibiaxial elongation data for end-linked PDMS networks in which trapped entanglements were dominant in number relative to chemical crosslinks. The parameter κ was used as an empirical fitting parameter, and the best-fit procedure yielded $\kappa = 2.9$. The structural parameters (ν, ξ, μ, f) were estimated from the stoichiometry using the Miller–Macosko model [56] in conjunction with the measured sol fraction. They concluded that the diffused constraint model successfully reproduced the reduced stress–strain data over a wide range of deformations, but the model underestimated the modulus, G, because it did not consider trapped entanglements as additional crosslinks contributing to G. The theoretical value of G calculated using $\kappa = 2.9$ was approximately one order of magnitude smaller (G=5.22 kPa) than the experimental value (G=64.9 kPa).

TABLE 29.2 *Mooney–Rivlin parameters of the stress–strain isotherms for different networks systems [114].*

Polymer	Diluent	f	Crosslinker	T (°C)	φ	$2C_1$ (MPa)	$2C_1 + 2C_2$ (MPa)
PDMS	Lin. PDMS	4	γ-Irradiation	30	1.00	0.0304	0.0571
					0.80	0.0298	0.0476
					0.60	0.0299	0.0433
					0.40	0.0305	0.0398
PDMS	Lin. PDMS	4	γ-Irradiation	30	1.00	0.0218	0.0533
					0.80	0.0220	0.0365
					0.60	0.0218	0.0324
					0.40	0.0208	0.0290
PDMS	Lin. PDMS	4	γ-Irradiation	30	1.00	0.0118	0.0364
					0.80	0.0121	0.0255
					0.60	0.0117	0.0230
					0.40	0.0126	0.0168
PBD-S[a]	1,2,4-Trichlorobenzene	4	1% Sulfur	25	1.00	0.203	0.406
					0.80	0.202	0.343
					0.60	0.202	0.302
					0.40	0.196	0.272
					0.20	0.204	0.254
PBD-G	1,2,4-Trichlorobenzene	4	γ-Irradiation	10	1.00	0.0904	0.280
					0.80	0.0864	0.210
					0.60	0.0915	0.167
					0.40	0.0933	0.135
					0.20	0.0878	0.117
		24		10	1.00	0.0904	0.28
					0.80	0.0868	0.210
					0.60	0.0915	0.167
					0.40	0.0933	0.135
					0.20	0.0878	0.117
PBDG-P	1,2,4-Trichlorobenzene	4	1% BPO	10	1.00	0.142	0.228
					0.80	0.140	0.178
					0.60	0.138	0.160
					0.40	0.138	0.150
					0.20	0.142	0.144
		24		10	1.00	0.164	0.168
					0.80	0.140	0.178
					0.60	0.138	0.160
					0.40	0.138	0.150
					0.20	0.135	0.144
PIB	1,2,4-Trichlorobenzene	4	Disulfide	30	1.00	0.072	0.159
					0.80	0.083	0.103
					0.60	0.074	0.0953
					0.40	0.073	0.0777
				20	1.00	0.113	0.165
					0.80	0.0976	0.148
					0.60	0.104	0.131
					0.40	0.0905	0.115
				15	1.00	0.128	0.194
					0.80	0.123	0.170
					0.60	0.114	0.145
					0.40	0.108	0.114
POE	Phenylacetate	3	Triisocyanate	25	1.00	0.744	0.934
					0.597	0.660	0.795
					0.565	0.613	0.722
					0.488	0.575	0.732
					0.390	0.593	0.715
POE	Phenylacetate	3	Triisocyanate	25	0.429	0.251	0.320
					0.325	0.231	0.296
					0.220	0.263	0.266

TABLE 29.2 *Continued*

Polymer	Diluent	f	Crosslinker	T (°C)	φ	$2C_1$ (MPa)	$2C_1 + 2C_2$ (MPa)
POE	Phenylacetate	3	Triisocyanate	25	0.457	0.280	0.390
					0.341	0.329	0.402
					0.291	0.310	0.348
POP	Benzene		Tris(*p*-phenylisocyanate)	60	0.216	0.322	0.423
					0.216	0.328	0.477
			$M_c = 3{,}000$		0.286	0.450	0.546
			$M_c = 2{,}000$		0.286	0.448	0.594
					0.273	0.398	0.537
			$M_c = 1{,}025$		0.406	0.839	0.899
					0.421	0.839	0.859
			$M_c = 725$		0.464	0.810	0.835
					0.456	0.847	0.851
			$M_c = 730$		0.473	0.779	0.785
					0.477	0.796	0.832
					0.440	0.814	0.817
			$M_c = 740$		0.522	0.723	0.776
					0.519	0.647	0.713
			$M_c = 725$		0.480	0.861	0.959
					0.510	0.891	0.904

It should be noted that the effect of G is cancelled when reduced stress–strain data are analyzed. This explains the success of this model in describing the shape of the experimental curves. On the basis of the diffused constraint theory a detailed comparison between theory and experiment on swollen polymer networks has not yet been made.

TABLE 29.3. *Parameters of the stress–strain isotherms calculated from the Flory–Erman model for unswollen PDMS model networks[115].*

M_n(g mol^{-1})	f	$[f^*]_{ph}$(MPa)	κ	$2C_1$(MPa)	$2C_2$(MPa)
32,900	3	0.013	19.4	0.033	0.034
25,600	3	0.014	18.2	0.043	0.052
18,500	3	0.021	15.0	0.066	0.061
9,500	3	0.053	9.5	0.093	0.057
4,700	3	0.075	7.9	0.148	0.011
4,000	3	0.101	6.8	0.192	0.015
45,000	4	0.008	22.3	0.038	0.030
32,900	4	0.015	16.4	0.058	0.042
25,600	4	0.028	11.9	0.084	0.055
18,500	4	0.023	13.3	0.089	0.040
9,500	4	0.062	8.0	0.167	0.050
4,700	4	0.119	5.8	0.353	0.031
4,000	4	0.195	4.5	0.395	0.021
18,500	4	0.020	14.3	0.096	0.043
18,500	4	0.020	14.3	0.089	0.043
18,500	4	0.020	14.3	0.089	0.040
11,300	4	0.082	7.0	0.196	0.083
11,300	4	0.079	7.1	0.169	0.115
11,300	4	0.084	6.9	0.199	0.076
11,300	4	0.064	7.9	0.188	0.092
11,300	4	0.060	8.2	0.178	0.098
11,300	4	0.062	8.1	0.165	0.120
21,500	4	0.038	10.3	0.142	0.098
11,100	4	0.086	6.8	0.207	0.087
8,800	4	0.104	6.2	0.244	0.084

TABLE 29.4. *Parameters of the stress–strain isotherms for PDMS model networks calculated from the entanglement model (Eq. (29.46)) [54].*

M_n(g mol^{-1})	f	T(K)	$10^{-5}G$(Pa)	$10^{-5}(\nu RT)$(Pa)	T_e
32,900	3	298	0.699	0.286	0.467
25,600	3		0.947	0.377	0.474
18,500	3		1.27	0.508	0.467
9,500	3		1.50	1.41	0.641
4,700	3		1.59	2.00	0.467
4,000	3		2.07	2.66	0.536
45,000	4	298	0.68	0.185	0.278
32,900	4		1.00	0.335	0.38
25,600	4		1.40	0.618	0.571
18,500	4	298	1.29	0.517	0.324
9,500	4		2.17	1.38	0.466
4,700	4		3.84	2.63	0.439
4,000	4		4.16	4.185	0.625
18,500	4		1.35	0.45	0.278
11,300	4	298	2.79	1.72	0.744
11,300	4		2.84	1.68	0.723
11,300	4		2.75	1.77	0.769
11,300	4		2.75	1.50	0.804
11,300	4		2.76	1.41	0.752
11,300	4		2.85	1.44	0.771
21,600	4	298	2.40	0.871	0.774
11,100	4		2.94	1.87	0.866
8,800	4		3.28	2.28	0.783

29.3.3 Determination of the Model Parameters from Swelling Measurements

Swelling of elastomers in a solvent is a relatively simple technique for the characterization of polymer networks. Empirical information, such as the degree of swelling and the elastic modulus, can be obtained by direct measurements. Equilibrium swelling measurements and stress–strain measurements are the most frequently used methods for determining the relative degree of crosslinking. A quantitative analysis of the swelling data, however, requires further considerations.

According to the Frenkel–Flory–Rehner hypothesis the elastic and mixing contributions to the free energy are additive, and the mixing free energy for the network is the same as that of the corresponding uncrosslinked polymer. It follows from these assumptions that the thermodynamic activity of the solvent in the network contains two separable contributions, $a_{1,c}$ and $a_{1,u}$, representing the diluent activities in the crosslinked and the uncrosslinked polymers, respectively, and the ratio $a_{1,c}/a_{1,u}$ at identical concentrations yields the elastic component of the solvent activity. Experimental tests of this prediction have been performed by differential sorption measurements first conducted by

TABLE 29.5. *Network parameters calculated by the constrained chain (CC) and modified constrained chain (MCC) models [116,117].*

System	Crosslinker[a]	φ	$\xi kT/V_0$ (MPa)		κ_G	
			CC	MCC	CC	MCC
cis 1,4-	DCP 1.3%	0.197	0.312	0.325	1.1	0.9
Isoprene/	DCP 0.75%	0.165	0.215	0.220	1.6	1.6
benzene	DCP 0.30%	0.133	0.115	0.125	3.0	2.5
T=25 °C	DCP 0.20%	0.112	0.083	0.092	3.8	3.0
	DCP 0.10%	0.081	0.043	0.045	5.0	6.0
NR/*n*-decane	DCP	0.24–1.0	0.150	0.170	3.0	2.0
PEO/phenylac.	isocyanate	0.22–1.0	0.260	0.275	1.5	1.6
PBD/chl.benz.	sulfur	0.2–1.0	0.235	0.235	2.0	2.6
PDMS/benzene	el.radiation	0.32–1.0	0.125	0.135	2.5	2.0

[a]DCP: dicumyl peroxide.

Gee *et al.* [122]. In this experiment on natural rubber/benzene system the vapor pressure of the solvent and the amount of solvent absorbed by the crosslinked and uncrosslinked rubbers were determined simultaneously by using a sensitive microbalance housed in a vacuum system. Similar experiments were performed by Yen and Eichinger [6], Brotzman and Eichinger [7–9], Neuburger and Eichinger [10], Zhao and Eichinger [11] and McKenna *et al.* [13–16]. Conventionally the results of these measurements are given in term of the dimensionless swelling activity parameter [15] (or dilation modulus [6–11])

$$S = \lambda \ln (a_{1,c}/a_{1,u}). \tag{29.55}$$

Typical theoretical and experimental S vs. $\varphi^{-1/3}(=\lambda)$ curves are shown in Fig. 29.6. The phantom network theory predicts constancy while the affine network model predicts a monotonic increase of S with increasing $\varphi^{-1/3}$. Many of the experimental S vs. $\varphi^{-1/3}$ curves, including that of Gee *et al.* [122] exhibit a maximum. This behavior is consistent with the Flory–Erman theory, although the experimental peak is, in general, much sharper and of significantly greater magnitude than that predicted by the model. Neuburger and Eichinger [10] determined the swelling activity parameter for poly(dimethylsiloxane) networks in benzene and cyclohexane at 20 and 30 °C. They found that the benzene data at 20 °C can be reasonably well described by the Flory–Erman model with the parameters: $\xi/(N_A V_0) = 4.09\times 10^{-4}$ mol/cm^3, $\kappa = 1.0$, and $\zeta = 90$ (this value of ζ is much bigger than that required to fit the stress strain data). The value of the molecular weight between crosslinks, M_c, calculated from the equation $\xi/(N_A V_0) = \rho/2M_c$ was $M_c = 1{,}190$ g/mol. It is significantly smaller than the actual $M_c = 26{,}000$ g/mol. Even larger discrepancies were found between the calculated and the actual values of M_c for the PDMS/cyclohexane system. In this case the best fit was obtained using the phantom network model with $\xi/(N_A V_0) = 0.0012$ mol/cm^3 corresponding to $M_c = 406$ g/mol. The authors concluded that the deviation is the consequence of the breakdown of the Frenkel–Flory–Rehner theory, namely the hypothesis that the elastic and mixing free energies are separable.

McKenna *et al.* [13–16] performed similar investigations on natural rubber networks swollen in different diluents. They assumed that the elastic free energy contribution is adequately described by the phenomenological Valanis–Landel function (see Eq. (29.1)) and for the measured degree of swelling, they calculated it from the values of $w'(\lambda_s)$ determined in the unswollen state. Comparing these data with the mixing contribution obtained by using Eq. (29.24) they came to the conclusion that the value of the interaction parameter for the crosslinked polymer, χ_c, exceeds that of the solution of the uncrosslinked polymer, χ_u. This conclusion has been supported by lattice model calculations of Freed and Pesci [123], who pointed out that the effective interaction parameter depends on the crosslink density.

McKenna *et al.* [13–16] use the following relation for the swelling activity parameter:

$$S = \lambda \ln (a_{1,c}/a_{1,u}) = (\chi_c - \chi_u)\lambda^{-5} + V_1 w'(\lambda)/RT\lambda. \tag{29.56}$$

The important point to note from this equation is the assumption that $\chi_c = \chi_u$ often found in the use of the Frenkel–Flory–Rehner hypothesis, has been suppressed. Hence the first term on the right hand side of Eq. (29.56) provides insight into the thermodynamics of swelling and in particular is in accord with the experimental observation that $S \neq 0$ as $\lambda \to 1$, i.e., no swelling. A typical value for $\chi_c - \chi_u$ of

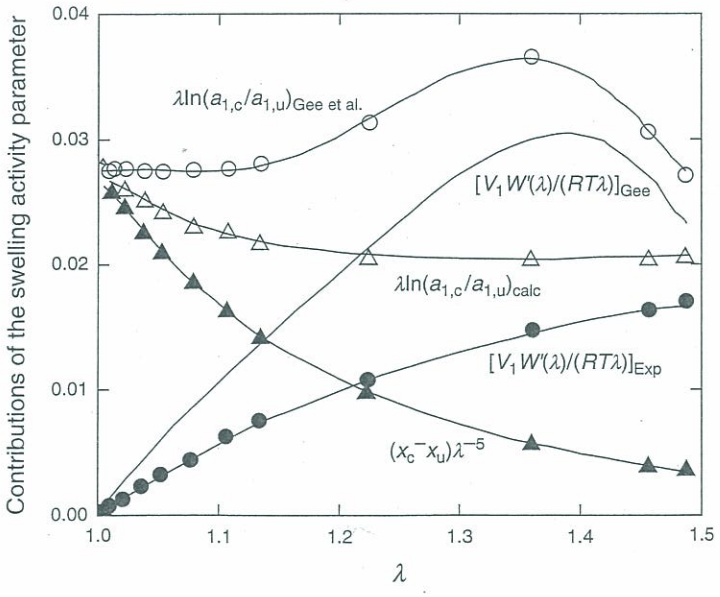

FIGURE 29.6. Thermodynamic parameters that contribute to the swelling activity parameter S vs. the swelling deformation $\lambda_s = \varphi^{-1/3}$. (After Ref. 15 see text for discussion).

0.027 can be obtained by examining the curve labeled $\lambda \ln (a_{1,c}/a_{1,u})_{\text{Gee et al.}}$ of Fig. 29.6 and taking the value at $\lambda = 1$.

In Fig. 29.6 we show the thermodynamic parameters from Eq. (29.56) and a comparison with the swelling data of Gee *et al* [122]. The curve labeled $\lambda \ln (a_{1,c}/a_{1,u})_{\text{Gee et al.}}$ refers to the data obtained by Gee *et al.* for S. The curve labeled $\lambda \ln (a_{1,c}/a_{1,u})_{\text{calc}}$ refers to a calculation of S from Eq. (29.56) using the values of $(\chi_c - \chi_u)\lambda^{-5}$ depicted in the plot on the curve so labeled summed with the values of $[V_1 w'(\lambda)/RT\lambda]_{\text{Exp}}$ determined experimentally by measurements on a rubber similar to that used by Gee *et al.* [122] and depicted with solid circles. The solid line without points labeled $[V_1 w'(\lambda)/RT\lambda]_{\text{Gee}}$ represents the value of the elastic contribution that would have been needed to have in order to agree with the Gee *et al.* [122] results for S, i.e., when added to the measured values of $(\chi_c - \chi_u)\lambda^{-5}$. The deviation between the measured and calculated curves is significant, i.e., the crosslink dependence of the interaction parameter does not provide an adequate explanation for the anomalous behavior of the swelling activity parameter. The reader is referred to McKenna *et al.* [13–16] for further discussion.

McKenna and Crissman [16] also investigated the effect of temperature on the shape of the S vs. $\varphi^{-2/3}(=\lambda^2)$ curves. In the polyisoprene/benzene system they did not observe a maximum in S at 30 and 40 °C, rather a rapid decrease occurred which was followed by a plateau region above $\lambda^2 = 1.2$. At 50 °C, however, a pronounced maximum was found at $\lambda^2 = 1.13$. Neuburger and Eichinger [10] reported similar changes in the swelling behavior for the PDMS/benzene system in the temperature range between 20 and 30 °C. Similar results were reported for changing solvent quality by Zhao and Eichinger [11]. Such abrupt changes in behavior imply significant changes in the free energy of the network over a narrow range of temperatures (or solvent qualities). None of the existing network theories predicts such a possibility.

Sivasailam and Cohen [124] studied the effect of swelling on the elastic modulus of end-linked polydimethyl siloxane networks synthesized at the theta condition from a series of molecular weight precursors ($9{,}900 < M < 101{,}700$) at polymer concentrations from 100% to 40%. These networks exhibited a minimal number of defects as they were prepared from low polydispersity chains at an optimal ratio of crosslinks to precursor chains. The optimum ratio was chosen as the one that produced the network with the highest elastic modulus, the minimum equilibrium swelling, and the minimum soluble fraction. The wide range of precursor molecular weights allowed the investigation of the effect of trapped entanglements as a function of the molecular weight. Equilibrium swelling concentrations were determined in PDMS oligomer ($M_n = 3{,}900$ g/mol), and the elastic modulus was measured at three different states: in swelling equilibrium (fully swollen state), at the concentration at which the network was formed (reference state), and in the unswollen (dry) state (Table 29.6 and Table 29.7). The dependence of the modulus after cure, the dry modulus

TABLE 29.6. *Elastic modulus of end-linked PDMS networks made at different precursor concentrations [124,126].*

Molecular weight (g/mol)	Diluent	Volume fraction φ_{ref}	*Sol fraction w%	G_{ref} (kPa)
101,700		1.00	2.60	111
	PDMS	0.89	2.50	95
	oligomer	0.79	1.28	72
		0.74	2.10	62
		0.67	2.99	50
71,500		1.00	0.28	176
	PDMS	0.89	−1.41	143
	oligomer	0.78	−0.75	98
		0.49	−1.84	48
		0.40	−1.67	27
30,200		1.00	0.26	210
	PDMS	0.89	0.12	168
	oligomer	0.78	0.13	150
		0.70	−0.05	106
		0.59	−0.96	85
		0.50	−2.50	61
		0.40	−4.90	39
9,900		1.00	0.25	343
	PDMS	0.89	−0.07	277
	oligomer	0.80	−0.05	251
		0.69	−0.98	193
		0.57	−3.04	147
		0.51	−6.90	123

*The negative value indicates that solvent is expelled from the swollen network by syneresis. In these gels the amount of uncrosslinked polymer is practically negligible.

TABLE 29.7. *Experimental and calculated values of the elastic modulus of end-linked PDMS networks swollen in PDMS oligomer (M=3,900 g/mol, theta solvent) and in the dry state [124,126].*

Molecular weight (g/mol)	Polymer volume fraction		G_{sw} (kPa)		G_{dry} (kPa)	
	φ_{ref}	φ_θ	Exp.	Calc.	Exp.	Calc.
101,700	1.00	0.38	59	37	111	111
	0.89	0.37	62	32	105	87
	0.79	0.34	45	27	82	68
	0.74	0.32	36	23	71	60
	0.67	0.23	16	16	57	49
71,500	1.00	0.48	129	84	175	191
	0.89	0.44	110	70	148	150
	0.78	0.37	61	52	105	116
	0.50	0.30	36	29	77	51
30,200	1.00	0.51	153	121	210	229
	0.89	0.47	130	101	172	185
	0.78	0.45	109	87	159	148
	0.59	0.37	67	59	98	95
	0.50	0.33	48	48	72	74
9,900	1.00	0.62	280	258	342	363
	0.89	0.59	240	228	286	310
	0.80	0.56	212	203	263	270
	0.69	0.52	161	175	208	226
	0.57	0.47	133	141	172	182

after solvent extraction, and the degree of equilibrium swelling on precursor concentration during cure were compared to scaling predictions. The experimental scaling exponents were found to be strong functions of the molecular weight of the precursor chains and for high molecular weight precursors their values approached the theoretical prediction by Obukhov *et al.* [125] for entanglement-dominated networks. The authors concluded that for networks made of high molecular weight chains a major contribution to the modulus is from trapped entanglements. They also pointed out that at molecular weights below the entanglement molecular weight the modulus of the network is affected by the mutual interpenetration of interspersed chains.

The data of Sivasailam and Cohen were reanalyzed by Graessley [126] in terms of the entanglement model. According to this model the shear modulus at the reference state G_{ref} is the sum of crosslink and entanglement contributions

$$G_{ref} = \nu_{ref} kT + T_0 G_N^0 \varphi_{ref}^{2.3}, \tag{29.57}$$

where G_N^0 is the plateau modulus of the polymer melt (for PDMS $G_N^0 = 0.2\,MPa$), T_0 is the entanglement trapping factor, and φ_{ref} is the volume fraction of the polymer at crosslinking. Assuming that the first term (crosslink contribution) in Eq. (29.57) varies with the concentration as in the phantom network, and the second term (entanglement contribution) varies like the Mooney–Rivlin term C_2, the following equations can be derived

$$G_{ref} = G_0 \varphi_{ref} + T_0 G_N^0 \varphi_{ref}^{2.3}, \tag{29.58a}$$

$$G_{swollen} = G_0 \varphi_{ref}^{2/3} \varphi^{1/3} + T_0 G_N^0 \varphi_{ref} \varphi^{1.3}, \tag{29.58b}$$

$$G_{dry} = G_0 \varphi_{ref}^{2/3} + T_0 G_N^0 \varphi_{ref}^{2.3}, \tag{29.58c}$$

where $G_0 (= \nu kT)$ is the crosslink contribution in the dry state (this excludes trapped entanglement effects). Using Eqs. (29.58a–c) in conjunction with empirically obtained data for T_0 and the sol fraction, the elastic moduli of these gels were calculated (Table 29.7). No systematic deviation can be observed between the predicted and measured moduli.

Urayama *et al.* [127,128] made similar investigations on end-linked PDMS networks cross-linked in solution. The elastic moduli of gels made from M=29,400g/mol and M=4,400 g/mol precursor chains were measured in the fully swollen state in toluene (good solvent), and in the reference state (Table 29.8). The sol fraction of these gels was less than 10%. The same analysis described above indicates that at high polymer volume fractions the calculated and experimental values agree fairly well, while at high swelling ratios the deviation is pronounced [126]. The discrepancy may be the consequence of structural and chemical changes accompanied by the crosslinking process.

In general, the reasonable agreement between the predicted and measured values of the elastic modulus suggests that the effect of swelling on the elastic properties can be approximated as a sum of two distinct contributions: one due to the chemical crosslinks and the other due to the entanglements. The latter in polymer melts is independent of chain lengths and represent an entanglement contribution

TABLE 29.8. *Elastic modulus and polymer volume fraction of end-linked PDMS networks at the preparation state and in the fully swollen state in toluene (good solvent) [127,128].*

Molecular weight (g/mol)	Diluent	Polymer volume fraction		G_{ref} (kPa)	G_{sw} (kPa)
		φ_{ref}	φ_{sw}		
29,400	toluene	1.0	0.187	113	33
		0.852	0.155	93	27
		0.709	0.126	63	17
		0.544	0.093	30	73
		0.411	0.078	19	47
		0.281	0.055	9	2.3
		0.179	0.038	3	0.9
4,400	toluene	1.0	0.275	680	251
		0.777	0.216	423	149
		0.654	0.208	330	137
		0.601	0.194	297	119
		0.584	0.195	301	113
		0.504	0.180	241	100
		0.381	0.140	150	53
		0.298	0.109	61	29

when the network is formed. [126] Chemical crosslinks trap a fraction of this contribution into the structure that governs the elastic response of the network.

29.3.4 Analysis of the Experimental Results on the Basis of the Scaling Theory

The validity of scaling laws has been tested on several swollen network systems (Table 29.9). Munch *et al.* [99] studied the concentration dependence of the shear modulus for polystyrene model networks synthesized by copolymerization of styrene and divinylbenzene and swollen to equilibrium in benzene (good solvent for polystyrene). It was found that the modulus obeys a scaling law with equilibrium concentration, similar to that obtained for semidilute polymer solutions. The best fit to the equation $G = B\varphi_e^n$ yields B=4,200 kPa and n=2.28. Hild *et al.* [129] compared the concentration dependence of the shear moduli of poly(ethylene oxide) networks crosslinked by aliphatic pluriisocyanate in two diluents: dioxane and water. The corresponding scaling laws were found: $G = 8{,}430\varphi_e^{2.30}$ kPa (in 1,4-dioxane) and $G = 10{,}400\varphi_e^{2.51}$ kPa (in water). The exponent obtained in 1,4-dioxane is in excellent agreement with the prediction of the scaling theory. However, for the same networks swollen in water a significantly higher exponent, n=2.51, was obtained. They assumed that the deviation from the theoretical exponent is due to the insolubility of the urethane linkages in water, which may induce inhomogeneities in the gels at the molecular level. Hecht and Geissler [130] investigated the elastic properties of polyacryamide gel homologs in a theta solvent (water–methanol mixture, 3:1 by volume). They found that in the concentration range $0.07<\varphi<0.3$ the longitudinal elastic modulus, E_L, obtained

TABLE 29.9. *Power law exponents for the concentration dependence of the elastic modulus in swollen network homologs.*

System	T (°C)	φ	A (kPa)	n	r	Ref.
NR/*n*-decane	20	0.06–0.40	4,500	2.06	0.992	[139, 140]
PS/benzene	20	0.05–0.20	4,200	2.28	0.955	[99]
PS/benzene	25	0.05–0.50	4,140	2.35	0.993	[99]
PS/cyclohexane	37	0.12–0.28	1,750	3.14	0.980	[28]
PEO/dioxane	25	0.03–0.35	8,430	2.30	0.984	[129]
PEO/water	25	0.03–0.30	10,401	2.51	0.992	[129]
PHPMA	25	0.08–0.35	2,590	2.59	0.995	[129]
PDMS/toluene	25	0.10–0.40	2,650	2.20	0.988	[23]
PVAC/toluene	25	0.06–0.30	2,430	2.27	0.990	[22]
PVAC/acetone	25	0.05–0.25	4,420	2.25	0.992	[22]
PVAC/isopropanol	70	0.10–0.60	3,388	2.31	0.977	[132]
PAA/water	25	0.03–0.30	4,880	2.23	0.991	[141]
PVA/water	25	0.03–0.30	3,500	2.11	0.993	[139]

NR: natural rubber; PS: polystyrene; PEO: poly(ethylene oxide); PHPMA: poly(hydroxi-ethyl-methacrylate); PDMS: polydimethylsiloxane; PVAC: poly(vinyl acetate); PAA: poly(acryamide); PVA: poly(vinyl alcohol); r: correlation coefficient.

from light scattering observations, obeys a scaling law $E_L = 8.090\varphi_e^{3.07}$ kPa in reasonable agreement with the theoretical prediction. Richards and Davidson [131] determined the shear moduli of randomly crosslinked polystyrene networks swollen in cyclohexane at the theta (Θ) temperature and also in toluene (good solvent condition). The power law exponent, n=3.7, reported for the theta system exceeds that of the theoretical value. In good solvent condition (toluene, 20 °C) they found the value n=2.25. A comprehensive study of the dependence of the elastic (shear) modulus on the polymer concentration was performed by Zrínyi and Horkay [132] on poly(vinyl acetate) gels swollen to equilibrium in isopropylalcohol. The thermodynamic quality of the solvent was varied by changing the temperature in the range from 30 °C to 70 °C. Isopropylalcohol is a theta solvent for poly(vinyl acetate) at 52°C and a good solvent at 70 °C. It was found that G vs. φ exhibits a simple power law behavior at each temperature. The exponent n varies between the values of 2.32 (good solvent condition, 70 °C) and 14.1 (poor solvent condition, 30 °C) [133]. At the theta temperature (52 °C) the best fit to the experimental data yields n=3.10.

The osmotic response of swollen polymeric networks was studied on the basis of the scaling theory by Horkay *et al.* [17–19,22,23,133]. They measured both the swelling pressure, ω, and the shear modulus of gels, G, at different stages of dilution. The swelling pressure vs. polymer volume fraction data were analyzed according to the equation [22]

$$\omega = \Pi - G = A\varphi^n - G_v^e(\varphi/\varphi_e)^m, \qquad (29.59)$$

where Π is the "osmotic" pressure of the swollen network and G_v^e is the value of the volume elastic modulus at equilibrium with the pure solvent ($\omega = 0$) and the constant A depends on the polymer/solvent system. The exponents n and m were iteratively adjusted to minimize the variance of ω for each set of data points. The resulting values of A, n, m, and G_v^e for poly(vinyl acetate) gels are displayed in Table 29.10. The n values are consistent with the scaling prediction for the mixing term. Also displayed in Table 29.10 are the values of the shear modulus, G_s^e, measured at the swelling equilibrium condition. The agreement between the numerical values of the shear and the volume elastic moduli provides experimental evidence that in highly swollen networks the separability of the elastic and mixing terms is a reasonable approximation.

29.4 SUMMARY

A survey of the thermodynamics and mechanics of crosslinked gels has been presented. Subjects include the phenomenological description of crosslinked networks within the framework of finite elasticity theory and continuum thermodynamics. Particular emphasis is placed on the Valanis–Landel form of the strain energy density function. Several statistical mechanical models of rubber elasticity are also presented. Of particular usefulness are the affine and phantom network models, which are commonly used to derive information about the molecular parameters of the gel from swelling or mechanical measurements. Techniques for using these models and the more modern Flory–Erman constrained junction model and its most recent modifications are described. Experimental data from the literature are presented and used to deduce molecular parameters for the networks using the different models. The application of Scaling Theory to polymer gels is also considered.

ACKNOWLEDGMENTS

FH acknowledges the support of the Intramural Research Program of the NIH, NICHD. GBM would like to acknowledge the support of the National Science Foundation for partial support of this work under grant DMR-0307084. We also thank J. Wang for help with the figures.

TABLE 29.10. *Swelling pressure and shear modulus parameters of PVAc networks in toluene and acetone [22].*

Sample	φ_e	A	n	m	G_v^e(kPa)	G_s^e(kPa)
Toluene 25 °C						
3/50	0.089	2171	2.28	0.342	8.6	8.9
6/50	0.146	2613	2.29	0.331	31.6	32.4
6/200	0.078	2072	2.22	0.340	7.2	6.9
9/50	0.208	2481	2.27	0.355	70.8	70.3
9/100	0.141	2350	2.25	0.336	28.6	28.3
9/200	0.112	2374	2.27	0.326	16.6	16.7
9/400	0.074	2273	2.27	0.315	6.16	6.26
12/50	0.229	3100	2.35	0.383	95.7	99.8
12/200	0.133	2425	2.26	0.335	25.5	25.2
Acetone 25 °C						
9/100	0.103	4264	2.24	0.321	24.9	25.9
9/200	0.078	4731	2.26	0.346	14.9	14.8
9/400	0.051	4262	2.24	0.369	5.44	5.24

REFERENCES

1. Guth, E. and Mark, H. *Monatshefte*, **65**, 93 (1934).
2. Flory, P.J. and Rehner, J. *J. Chem. Phys.*, **11**, 521 (1943).
3. James, H.M. and Guth, E. *J. Chem. Phys.*, **15**, 651 (1947).
4. Flory, P.J. *Principles of Polymer Chemistry*; Cornell University. Press, Ithaca, NY, 1953.
5. Frenkel, J. *Rubber Chem. Technol.*, **13**, 264 (1940).
6. Yen, L.Y. and Eichinger, B.E. *J. Polym. Sci. Polym. Phys. Ed.* **16**, 121 (1978).
7. Brotzman, R.W and Eichinger, B.E. *Macromolecules* **14**, 1445 (1981).
8. Brotzman, R.W. and Eichinger, B.E. *Macromolecules* **15**, 531 (1982).
9. Brotzman, R.W. and Eichinger, B.E. *Macromolecules* **16**, 1131 (1983).
10. Neuburger, N.A. and Eichinger, B.E. *Macromolecules* **21**, 3060 (1988).
11. Zhao, Y. and Eichinger, B.E. *Macromolecules* **25**, 6988 (1992).
12. Gottlieb, M. and Gaylord, R.J. *Macromolecules* **17**, 2024 (1984).
13. McKenna, G.B., Flynn, K.M. and Chen, Y. *Polym. Commun.* **29**, 272 (1988).
14. McKenna, G.B., Flynn, K.M. and Chen, Y. *Macromolecules* **22**, 4507 (1989).
15. McKenna, G.B., Flynn, K.M. and Chen, Y. *Polymer* **31**, 1937 (1990).
16. McKenna, G.B. and Crissmann, J.M. *J. Polym. Sci B. Polym. Phys.* 35, 817 (1997).
17. Horkay, F. and Zrinyi, M. *Macromolecules*, **15**, 1306 (1982).
18. Horkay, F. and Zrinyi, M. *J. Macromol. Sci. Phys.* **B25**, 307 (1986).
19. Horkay, F., Geissler, E., Hecht, A.M. and Zrinyi, M. *Macromolecules*, **21**, 2589 (1988).
20. Geissler, E., Horkay, F., Hecht, A.M. and Zrinyi, M. *J. Chem. Phys.* **90**, 1924 (1989).
21. Horkay, F., Hecht, A.M. and Geissler, E. *Macromolecules*, **22**, 2007 (1989).
22. Horkay, F., Hecht, A.M. and Geissler, E. *J. Chem. Phys.* **91**, 2706 (1989).
23. Horkay, F., Zrinyi, M., Geissler, E., Hecht, A.M. and Pruvost, P. *Polymer*, **32**, 835 (1991).
24. Horkay, F., Hecht, A.M., Mallam, S., Geissler, E. and Rennie, A.R. *Macromolecules*, **24**, 2896 (1991).
25. Hecht, A.M., Horkay, F., Geissler, E. and Benoit, J.P. *Macromolecules*, **24**, 4183 (1991).
26. Geissler, E., Horkay, F. and Hecht, A.M. *Macromolecules*, **24**, 6006 (1991).
27. Hecht, A.M., Guillermo, A., Horkay, F., Mallam, S., Legrand, J.F. and Geissler, E. *Macromolecules*, **25**, 3677 (1992).
28. Hecht, A.M., Horkay, F., Mallam, S. and Geissler, E. *Macromolecules*, **25**, 6915 (1992).
29. Horkay, F., Burchard, W., Geissler, E. and Hecht, A.M. *Macromolecules*, **26**, 1296 (1993).
30. Horkay, F., Burchard, W., Hecht, A.M. and Geissler, E. *Macromolecules*, **26**, 3375 (1993).
31. Geissler, E., Horkay, F. and Hecht, A.M. *Phys.Rev.Lett.* **71**, 645 (1993).
32. Douglas, J.F. and McKenna, G.B. *Macromolecules*, **26**, 3282 (1993).
33. Flory, P.J. and Tatara, Y. *J. Polym. Sci., Polym. Phys. Ed.*, **13**, 683 (1975).
34. Ronca, G. and Allegra, G. *J. Chem. Phys.*, **63**, 4990 (1975).
35. Flory, P.J. *Proc. R. Soc. Lond.* **A351**, 351 (1976).
36. Flory, P.J. *J. Chem. Phys.*, **66**, 5720 (1977).
37. Erman, B. Wagner, W. and Flory, P.J. *Macromolecules* **13**, 1554 (1980).
38. Flory, P.J. and Erman, B. *Macromolecules* **15**, 800 (1982).
39. Erman, B. and Flory, P.J. *Macromolecules* **15**, 806 (1982).
40. Erman, B. and Flory, P.J. *Macromolecules* **16**, 1600 (1983).
41. Mark, J.E. *Adv. Polym. Sci.*, **44**, 1 (1982).
42. Queslel, J.P. and Mark, J.E. *J. Polym. Sci., Polym. Phys. Ed.* 22, 49 (1984).
43. Queslel, J.P. and Mark, J.E. *Adv. Polym. Sci.*, **65**, 135 (1984).
44. Queslel, J.P. and Mark, J.E. *Adv. Polym. Sci.* **71**, 229 (1985).
45. Langley, N.R. *Macromolecules* **1**, 348 (1968).
46. Dossin, L.M. and Graessley, W.W. *Macromolecules* **12**, 123 (1979).
47. Pearson, D.S. and Graessley, W.W. *Macromolecules* **11**, 528 (1978).
48. Pearson, D.S. and Graessley, W.W. *Macromolecules* **13**, 1001 (1980).
49. Graessley, W.W. *Adv. Polym. Sci.*, **47**, 67 (1982).
50. Marucci, G. *Rheol. Acta* **18**, 193 (1979).
51. Marucci, G. *Macromolecules* **14**, 434 (1981).
52. Gottlieb, M. and Gaylord, R.J. *Polymer* **24**, 1644 (1983).
53. Gottlieb, M., Macosco, C.W. and Lepsch, T.C. *J. Polym. Sci., Polym. Phys. Ed.* **19**, 1603 (1981).
54. Gottlieb, M., Macosco, C.W., Benjamin, G.S., Meyers, K.O. and Merrill, E.W. *Macromolecules* **14**, 1039 (1981).
55. Gottlieb, M. and Macosco, C.W. *Macromolecules* **15**, 535 (1982).
56. Miller, D.R. and Macosco, C.W. *Macromolecules* **9**, 206 (1976).
57. Gaylord, R.J. and Douglas, J.F. *Polym. Bull.* **23**, 529 (1990).
58. Rivlin, R.S. *Philos. Trans. R. Soc.* **A241**, 379 (1948).
59. Treloar, L.R.G. *The Physics of Rubber Elasticity*, Clarendon, Oxford, 1975.
60. Valanis, K.C. and Landel, R.F. *J. Appl. Phys.*, **38**, 2997 (1967).
61. McKenna, G.B. and Hinkley, J.A. *Polymer* **27**, 1368 (1986).
62. Kearsley, E.A. and Zapas, L.J. *J.Rheol.* **24**, 483 (1980).
63. Jones, D.F. and Treloar, L.R.G. *J. Phys. D. (Appl. Phys.)* **8**, 1285 (1975).
64. Mooney, M. *J. Appl. Phys.*, **11**, 582 (1940).
65. Flory, P.J. *Chem. Rev.* 35, 51 (1944).
66. Vega, D.A., Villar, M.A., Alessandrini, J.L. and Valles, E.M. *Macromolecules*, **34**, 4591 (2001).
67. Edwards, S.F. and Muller-Nedebock, K.K. *J. Phys. A—Math. Gen.*, **32**, 3301 (1999).
68. Sommer, J.U., Vilgis, T.A. and Heinrich, G. *J. Chem. Phys.*, **100**, 9181 (1999).
69. Ryzmski, W.M. and Walska, B. *Polimery*, **48**, 246 (2003).
70. Graessley, W.W. *Macromolecules* **8**, 186 (1975).
71. Horkay, F., McKenna, G.B., Deschamps, P. and Geissler, E. *Macromolecules*, **33**, 5215 (2000).
72. Jackson, C.L. and McKenna, G.B. *Rubber Chem. Technol.*, **64**, 760 (1991).
73. Madkour, T. and Mark, J.E. *Polym. Bull.*, **31**, 615 (1993).
74. Saalwachter, K., Kleinschmidt, F. and Sommer, J.U. *Macromolecules*, **37**, 8556 (2004).
75. Ball, R.C., Edwards, S.F. and Warner, M. *Polymer* **22**, 1010 (1981).
76. Ball, R.C. and Edwards, S.F. *Macromolecules* **13**, 748 (1980).
77. DiMarzio, E.A. *J. Chem. Phys.*, **36**, 1563 (1962).
78. DiMarzio, E.A. *Polymer* **35**, 1819 (1994).
79. Deam, R.T. and Edwards, S.F. *Philos. Trans. R. Soc. Lond., A*, **280**, 378 (1978).
80. Edwards, S.F. *Proc. Phys. Soc.*, **92**, 9 (1967).
81. Gaylord, R.J. and Douglas, J.F. *Polym. Bull.*, **18**, 347 (1987).
82. Edwards, S.F. and Vilgis, Th. *Polymer* **27**, 483 (1986).
83. Kilian, H.G. *Polymer* **22**, 209 (1982).
84. Enderle, H.F. and Kilian, H.G. *Prog. Colloid Polym. Sci.*, **75**, 55 (1987).
85. Gao, J. and Weiner, J.H. *Macromolecules* **20**, 2520 (1987).
86. Gao, J. and Weiner, J.H. *Macromolecules* **22**, 979 (1989).
87. Deloche, B. and Samulski, E.T. *Macromolecules* **21**, 3107 (1988).
88. Wall, F.T. *J. Chem. Phys.*, **11**, 527 (1943).
89. Flory, P.J. and Wall, F.T. *J. Chem. Phys.*, **19**, 1435 (1951).
90. Hermans, J.J. *Trans. Faraday Soc.* **43**, 591 (1947).
91. James, H.M. and Guth, E. *J. Chem. Phys.*, **15**, 669 (1947).
92. James, H.M. and Guth, E. *J. Chem. Phys.*, **21**, 1039 (1953).
93. Guth, E. *J. Polym. Sci., Pt. C*, **12**, 89 (1966).
94. Erman, B. and Monnerie, L. *Macromolecules* **22**, 3342 (1989).
95. Kloczkowski, A., Mark, J.E. and Erman, B. *Macromolecules* **28**, 5089 (1995).
96. Douglas, J.F. and McKenna, G.B. in *Elastomeric Polymer Networks*, edited by J.E. Mark and E. Burak, Prentice Hall, Englewood Cliffs, NJ, 1993.
97. Rubinstein, M. and Panyukov, S. *Macromolecules* **30**, 8036 (1997).
98. Doi, M. and Edwards, S.F. *The Theory of Polymer Dynamics*, Clarendon Press, Oxford, England, 1986.
99. Munch, J.P., Candau, S., Herz, J. and Hild, G. *J. Phys.*, **38**, 971 (1977).
100. Doi, M. *J. Polym. Sci., Polym. Phys. Ed.* **21**, 667 (1983).
101. Rubinstein, M. and Panyukov, S. *Macromolecules* **35**, 6670 (2002).
102. Muthukumar, M. and Edwards, S.F. *J. Chem. Phys.*, **76**, 2720 (1982).
103. Muthukumar, M. *J. Chem. Phys.*, **85**, 4722 (1986).
104. des Cloiseaux, J. *J. Phys. (Les Ulis)* **36**, 281 (1973).

105. de Gennes, P.G. *Scaling Concepts in Polymer Physics*, Cornell, Ithaca, NY, 1979.
106. Flory, P.J. *Discuss Faraday. Soc.*, **49**, 7 (1970).
107. Ferry, J.D. *Viscoelastic Properties of Polymers*, Wiley, New York, 1970.
108. Queslel, J.P., Fontaine, F. and Monnerie, L. *Polymer* **29**, 1086 (1988).
109. Erman, B. and Mark, J.E. *Macromolecules* **20**, 2892 (1987).
110. Erman, B. and Mark, J.E. *Macromolecules* **25**, 1919 (1992).
111. Han, W.H., Horkay, F. and McKenna, G.B. *Math. Mech. Solids*, **4**, 139 (1999).
112. Allen, G., Kirkham, M.J., Padget, J. and Price, C. *Trans. Faraday Soc.*, **67**, 1228 (1971).
113. Mark, J.E. and Sullivan, J.L. *J. Chem. Phys.*, **66**, 1006 (1977).
114. Brotzman, R.W. and Mark, J.E. *Macromolecules* **19**, 667 (1986).
115. Sharaf, M.A. and Mark, J.E. *Polymer* **35**, 740 (1994).
116. Fontaine, F., Morland, C., Noel, C., Monnerie, L. and Erman, B. *Macromolecules* **22**, 3348 (1989).
117. Fontaine, F., Noel, C., Monnerie, L. and Erman, B. *Macromolecules* **22**, 3352 (1989).
118. Pak, H. and Flory, P.J. *J. Polym. Phys.*, **17**, 1845 (1979).
119. Kawamura, T., Urayama, K. and Kohjiya, S. *Macromolecules*, **34**, 8252 (2001).
120. Urayama, K., Kawamura, T. and Kohjiya, S. *Macromolecules*, **34**, 8261 (2001).
121. Urayama, K., Kawamura, T. and Kohjiya, S. *J. Chem. Phys.*, **118**, 5658 (2003).
122. Gee, G., Herbert, J.B.M. and Roberts, R.C. *Polymer* **6**, 541 (1965).
123. Freed, K.F. and Pesci, A.I. *Macromolecules* **22**, 4048 (1989).
124. Sivasailam, K. and Cohen, C. *J. Rheol.*, **44**, 897 (2000).
125. Obukhov, S.P., Rubinstein, M. and Colby, R.H. *Macromolecules*, **27**, 3191 (1994).
126. Graessley, W.W. *Polymeric Liquids and Networks: Structure and Properties*, Garland Science, New York, 2004.
127. Urayama, K. and Kohjiya, S. *J. Chem. Phys.*, **104**, 3352 (1996).
128. Urayama, K., Kawamura, T. and Kohjiya, S. *J. Chem. Phys.*, **105**, 4833 (1996).
129. Hild, G., Okasha, R., Macret, M. and Gnanou, Y. *Makromol. Chem.* **187**, 2271 (1986).
130. Hecht, A.M. and Geissler, E. *J. Phys.* **39**, 631 (1978).
131. Richards, R.W. and Davidson, N.S. *Macromolecules* **19**, 1381 (1986).
132. Zrinyi, M. and Horkay, F. *Macromolecules* **17**, 2805 (1986).
133. Horkay, F. and Zrinyi, M. *Macromolecules* **21**, 3260 (1988).
134. Chiu, D.S. and Mark, J.E. *Colloid Polym. Sci.* **255**, 644 (1977).
135. Chiu, D.S., Su, T.K. and Mark, J.E. *Macromolecules* **10**, 1110 (1977).
136. Rahalkar, R.R. and Mark, J.E. *Polym. J. (Tokyo)* **12**, 835 (1980).
137. Sung, P.H. and Mark, J.E. *J. Polym. Sci. Polym. Phys. Ed.* **19**, 507 (1981).
138. Andrady, A.L. and Llorente, M.A. *J. Polym. Sci. Polym. Phys. Ed.* **25**, 507 (1987).
139. Horkay, F. and Zrinyi, M. *Polym. Bull.* **4**, 21, 361 (1981).
140. Bristow, G.M. *J. Appl. Polym. Sci.* **9**, 1571 (1965).
141. Geissler, E., Hecht, A.M., Horkay, F. and Zrinyi, M. *Macromolecules* **21**, 2594(1988).